



Qualitative assessment of PMIP3 rainfall simulations across the eastern African monsoon domains during the mid-Holocene and the Last Glacial Maximum

Manuel Chevalier ^{a,*}, Simon Brewer ^b, Brian M. Chase ^a

^a Centre National de la Recherche Scientifique, UMR 5554, Institut des Sciences de l'Evolution de Montpellier, Université de Montpellier, Bat. 22 CC061, Place Eugène Bataillon, 34095, Montpellier, Cedex 5, France

^b Geography Department, University of Utah, Salt Lake City, USA



ARTICLE INFO

Article history:

Received 27 May 2016

Received in revised form

19 October 2016

Accepted 22 November 2016

Available online 6 December 2016

Keywords:

Africa

Southern hemisphere

Palaeoclimate

Monsoon

Intertropical convergence zone

Data-model comparison

PMIP3

Mid-Holocene

Last Glacial Maximum

ABSTRACT

In this paper we compare a compilation of multiproxy records spanning the eastern African margin with general circulation model simulations of seasonal precipitation fields for the mid-Holocene and the Last Glacial Maximum (LGM) carried out as part of the third phase of the Paleoclimate Modelling Intercomparison Project (PMIP3). Results show good agreement during the mid-Holocene (the '6K experiment'), with palaeodata and model outputs correlating well and indicating that changes in insolation drove a stronger northern African monsoon (north of ~0–5°S) during the terminal "African Humid Period" and a weaker southeast African monsoon. For the LGM (the '21K experiment'), however, significant discrepancies exist both between model simulations, and between existing palaeodata and simulated conditions, both in terms of direction and amplitude of change. None of the PMIP3 simulations reflect the pattern inferred from the palaeodata. Two major discrepancies have been identified to explain this: 1) the limited sensitivity of the southern monsoon domain to the colder temperatures of the Indian Ocean (~2 °C), and 2) the absence of changes in the dynamic of the Indian Ocean Walker circulation over the entire basin, despite the exposure of the Sahul and Sunda shelves that weakened convection over the Indo-Pacific Warm Pool during the LGM. These results indicate that some major features of the atmospheric and oceanic teleconnections between the different monsoon regions require further consideration as models evolve.

© 2016 Elsevier Ltd. All rights reserved.

1. Introduction

Combined under the concept of the 'Global Monsoon', the Earth's tropical monsoon domains form a network of rainfall systems with similar sensitivities to external and internal climate forcing (Wang and Ding, 2008; Wang et al., 2014; Yim et al., 2014). Guo et al. (2012) argued that at orbital time-scales the Global Monsoon has two pacing components, one being related to the low-latitude summer insolation changes (anti-phase between the Northern and Southern hemispheres), and the other being modulated by glacial-interglacial cycles (synchronous changes in Northern and Southern hemispheres). The mid-Holocene (6000 cal BP, '6k') and Last Glacial Maximum (LGM, 21,000 cal BP, '21k')

experiments proposed by the Paleoclimate Modelling Intercomparison Project group (PMIP, Braconnot et al., 2004; Joussaume and Taylor, 1995) represent two end-member simulations to specifically assess how general circulation models (GCMs) deal with these two pacing components: the 6k experiment to assess the impact of insolation forcing, and the 21k experiment for global thermal forcings associated with changes in atmospheric greenhouse gases concentration, lower sea-level and the presence of large polar ice-sheets.

Extending from 35°S to 37°N, Africa encompasses both tropics, and hosts a northern and a southern monsoon domain. This makes it an ideal case study to test the performance of PMIP3/CMIP5 models (Braconnot et al., 2012; Harrison et al., 2015; Taylor et al., 2012) to simulate interhemispheric atmospheric and oceanic teleconnections that exist or have existed between: 1) northern and southern monsoon domains, and 2) tropical and mid- to high latitudes circulation systems. The hydroclimate of both monsoon

* Corresponding author.

E-mail address: manuel.chevalier@univ-montp2.fr (M. Chevalier).

domains is characterized by a strong seasonality driven by the seasonal north-south migration of the tropical rainbelt (sometimes conflated with the Intertropical Convergence Zone (ITCZ)) that roughly tracks the zone of maximum insolation (Donohoe et al., 2013; McGee et al., 2014; Schneider et al., 2014). Its annual double passage over equatorial Africa during the boreal spring and autumn seasons results in a bimodal rainfall seasonality between 5°S and 5°N with two rainfall peaks and the quasi-absence of rain-free months (Fig. 1C; Hastenrath, 2001).

Variability in African monsoon strength has long been a subject of considerable research interest (e.g. Harrison et al., 1998; Kutzbach, 1981; Prell and Kutzbach, 1987), with particular attention being given to the most recent period of maximum extension and intensity of the northern monsoon domain, the so-called African Humid Period (AHP), which took place between 14.8 and 5.5 ka *sensu* deMenocal et al. (2000) and caused a ‘greening’ of the Sahara (Claussen and Gayler, 1997). The AHP has been the focus of attention for a large part of the community studying its occurrence, spatial extent and timing (e.g. Braconnot et al., 2007b, 2000; Claussen et al., 2013, 2003; Coe and Harrison, 2002; Joussaume et al., 1999; Kutzbach and Street-Perrott, 1985; Kutzbach, 1981; Peyron et al., 2006). However, only a limited number of modelling and data-model comparison studies have dedicated consideration to the southern domain (e.g. Barker and Gasse, 2003; Otto-Bliesner et al., 2014; Pinot et al., 1999; Singarayer and Burrough, 2015). This asymmetry can be partly explained by the poor data coverage in Africa south of the Equator (Anderson et al., 1988; Bartlein et al., 2011) and the sometimes ambiguous climatic significance of some of the records available (see the regional syntheses of Burrough and Thomas (2013), Chase and Meadows (2007), Gasse et al. (2008) and Scott et al. (2012) and the references therein). However, recent work has presented many continuous and well-dated records from both East Africa (e.g. Bouimetarhan et al.,

2015; Castañeda et al., 2007; Garcin et al., 2012, 2009, 2006; Loomis et al., 2012; Sinnighe Damsté et al., 2011; Tierney and DeMenocal, 2013; Tierney et al., 2011a,b, 2008; Verschuren et al., 2009) and southern Africa (e.g. Baker et al., 2014; Chase et al., 2015a, 2015b, 2013, 2010, 2009, Chevalier and Chase, 2016, 2015; Lim et al., 2016; Neumann et al., 2010, 2008, 2014; Norström et al., 2014; Quick et al., 2015a, 2015b; Schefuß et al., 2011; Truc et al., 2013; Wang et al., 2013). These new records now provide the spatial data coverage required for robust data-model comparisons.

In this study, we will focus on comparing PMIP3 GCM rainfall simulations with a compilation of African palaeorecords (from 30°S to 15°N and east of 25°E, Fig. 1A, Table 1) that can be most reliably interpreted as proxies of palaeo-precipitation (as distinct from aridity (precipitation minus potential evapotranspiration, Chevalier and Chase, 2016)). From North to South, the study area encompasses the Horn of Africa, the African Rift, the lower Zambezi basin and the eastern part of southern Africa. Comparing GCM simulations of precipitation variability during the mid-Holocene and the LGM allows for an assessment of the models' ability to simulate past conditions and dynamics in tropical Africa and identify the relative influence of the Global Monsoon drivers on the northern and southern African monsoon domains during each period.

2. Material & methods

2.1. PMIP3/CMIP5 models

Palaeoclimate simulations provide a unique opportunity to test GCMs outside their calibration range and to evaluate their predictive power against non-analog boundary conditions (Braconnot et al., 2004; Harrison et al., 2015; McCarroll, 2015; Schmidt et al., 2014a). In PMIP experiments, models are run for hundreds of

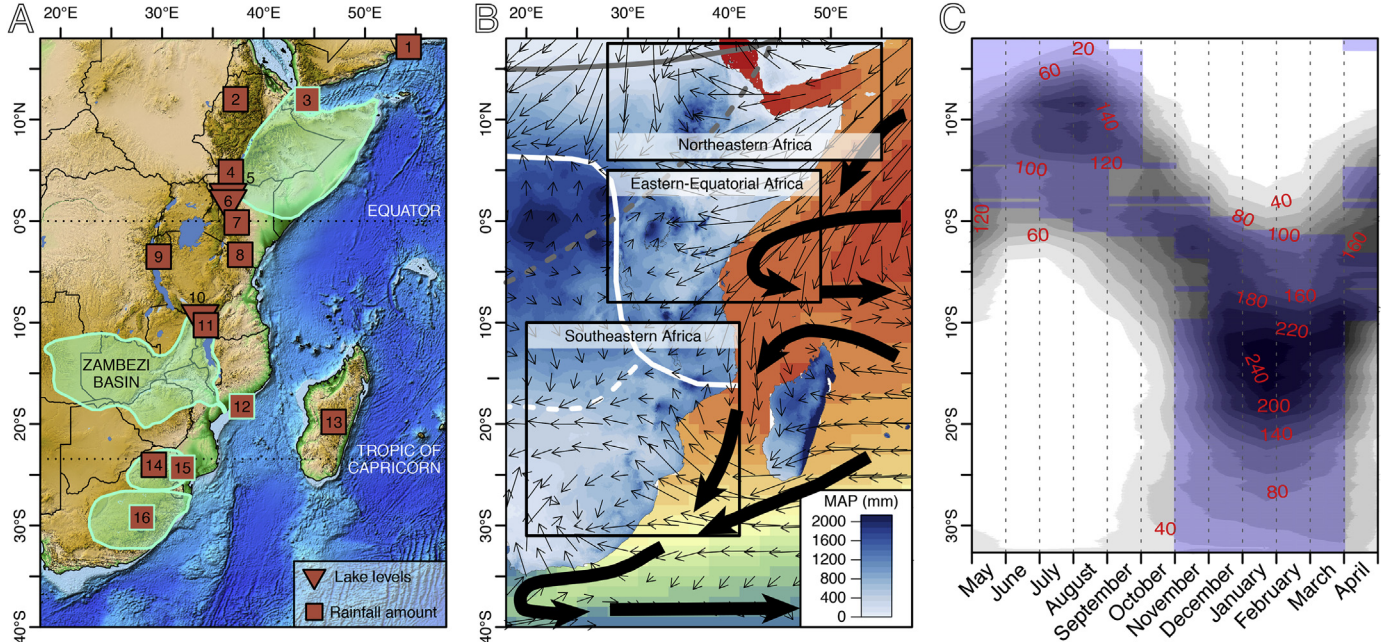


Fig. 1. A) Map of the topography of Africa (ETOPO1, Amante and Eakins, 2009). Red squares and triangles position the sites used in the comparison with model outputs. Exact coordinates, original reference and proxy used are summarized in Table 1. Green shading indicates the attraction basin of the associated records (3, 12, 15 and 16). B) Mean Annual Precipitation (MAP, Worldclim database, Hijmans et al., 2005) is represented in blue and austral summer SSTs (Reynolds et al., 2002) in red to green. Large black arrows represent the major oceanic currents while the small black arrows represent mean January windfield (NCEP/NCAR 40-years reanalysis project; Kalnay et al., 1996). The three boxes (northeastern, eastern-equatorial and southeastern Africa) are used to compute regional averages. C) Mean monthly rainfall (mm) at different latitudes averaged for the continental longitudes between 18°E and 58°E. Levels of grey represent different isohyets from low (white means less than 20 mm) to high (black means more than 240 mm) rainfall amount. The five consecutive wettest months are shaded in blue. (For interpretation of the references to colour in this figure legend, the reader is referred to the web version of this article.)

Table 1

List of the different sites (sorted from north to south) used to test the model. The last three columns indicate the average value with its standard deviation of the period considered (the last millennium, between 5.5 and 6.5 ka, and between 20 and 22 ka for the pre-Industrial period, the mid-Holocene and the LGM, respectively). Significativity of the 6k and 21k anomalies was tested with a Student t-test and the p-values are provided between parentheses.

#	Site Name	Lon. (°E)	Lat. (°N)	Reference	Proxy	Original Interpretation	PI	6K	21K
1	Qunf Cave	53.3	17.17	Fleitmann et al. (2003)	Speleothem δ _{18O} Speleothem δ _{18O}	Rainfall amount	−6.76 ± 0.28	−1.67 ± 0.33 (p < 10 ^{−9})	
2	Lake Tana	37.25	12	Marshall et al. (2011)	Ti XRF counts	Aridity	7.60 ± 0.38	9.11 ± 0.33 (p < 10 ^{−14})	
3	Gulf of Aden (marine core P178- 15P)	44.3	11.955	Tierney and DeMenocal (2013)	δD	Rainfall amount/ monsoon intensity	−132.8 ± 2.6	−143.7 ± 2.2 (p < 10 ^{−16})	−116.9 ± 1.4 (p < 10 ^{−19})
4	Lake Chew Bahir	36.78	4.84	Foerster et al. (2012)	K XRF counts	Aridity	4.11 ± 0.16 × 10 ³	2.52 ± 0.52 × 10 ³ (p < 10 ^{−8})	5.02 ± 0.34 × 10 ³ (p < 10 ^{−4})
5	Lake Turkana	35.5	2.6	Garcin et al. (2012)	Palaeoshorelines	Lake levels (Aridity)	374 ± 4	453 ± 5 (p < 10 ^{−37})	
6	Lake Suguta	36.5	2	Garcin et al. (2009)	Palaeoshorelines	Lake levels (Aridity)	0	201 ± 56 (p < 10 ^{−12})	
7	Mount Kenya	37.35	−0.15	Barker et al. (2001)	δ _{18O}	Aridity	25.7 ± 1.9	21.1 ± 4.9 (p < 10 ^{−3})	
8	Lake Challa	37.7	−3.32	Tierney et al. (2011a,b)	δD	Rainfall amount	−104.3 ± 2.9	−113.7 ± 4.3 (p < 10 ^{−9})	−111.1 ± 3.8 (p < 10 ^{−10})
9	Burundi Highlands	29.67	−3.5	Bonneville and Chalié (2000)	Pollen-based reconstructions	Rainfall amount	24 ± 160	14 ± 38 (p = 0.79)	−459 ± 188 (p < 10 ^{−13})
10	Lake Masoko	33.76	−9.33	Garcin et al. (2006)	Magnetic Susceptibility	Lake levels (Aridity)	7.99 ± 1.07 × 10 ^{−6}	8.41 ± 1.48 × 10 ^{−6} (p = 0.30)	3.28 ± 1.02 × 10 ^{−6} (p < 10 ^{−18})
11	Lake Malawi	34.11	−10.01	Konecky et al. (2011)	δD	Rainfall amount	−105.0 ± 2.1	−97.5 ± 2.6 (p < 10 ^{−2})	−111.9 ± 1.7 (p < 10 ^{−3})
12	Zambezi River mouth (marine cores GIK16160-3 and GeoB9307-3)	37.87	−18.24	Wang et al. (2013)	δD	Rainfall amount	−154.3 ± 0.6	−152.1 ± 0.11 (p < 10 ^{−11})	−163.1 ± 1.8 (p < 10 ^{−33})
		37.38	−18.57	Schefuss et al. (2011)			−154.5 ± 2.3	−149.2 ± 2.3 (p < 10 ^{−6})	
13	Lake Tritrivakely	46.92	−19.78	Gasse and van Campo (2001)	Pollen-based correspondence analysis (CA)	Rainfall amount	60.8 ± 16.0	45.0 ± 1.5 (p < 10 ^{−2})	53 ± 0.9 (p < 10 ^{−8})
14	Cold Air Cave	29.18	−24.02	Holmgren et al. (2003)	Speleothem δ _{18O}	Rainfall amount	−4.47 ± 0.72	−4.07 ± 0.42 (p = 0.04)	−3.16 ± 0.3 (p < 10 ^{−7})
15	South Africa northern precipitation stack	32	−24.3	Chevalier and Chase (2015)	Pollen-based reconstructions	Rainfall amount	23.4 ± 10.1	17.5 ± 4.8 (p = 0.014)	−117.7 ± 14.2 (p < 10 ^{−43})
16	South Africa southern precipitation stack	28	−29.2	Chevalier and Chase (2015)	Pollen-based reconstructions	Rainfall amount	−16.5 ± 13.8	16.8 ± 3.4 (p < 10 ^{−9})	−102.2 ± 12.5 (p < 10 ^{−23})

years with pre-defined stable boundary conditions. The last decades of simulation are saved and taken to represent the equilibrium climate state of the period being considered. We only used the latest generation of PMIP experiments (PMIP3; Braconnot et al., 2012; Harrison et al., 2015), which are now part of the Coupled Model Intercomparison Project phase 5 (CMIP5, Taylor et al., 2012). PMIP3 differs from PMIP2 (Braconnot et al., 2007a, 2007b) with slightly tuned boundary conditions and improved spatial resolution of the different models (Braconnot et al., 2012). The PMIP3/CMIP5 protocol imposes the mid-Holocene and LGM boundary conditions to promote: 1) the direct comparison of model outputs, and 2) the derivation of ensemble models, which have the strong advantage of averaging out discrepancies found in individual simulations that result from different model parameterizations (Annan and Hargreaves, 2011, 2010; Hargreaves et al., 2013; IPCC, 2010; Knutti et al., 2010).

Mid-Holocene conditions differ from pre-industrial (PI) period conditions primarily through their orbital configuration and a reduced concentration of atmospheric methane (Table 2). This orbital configuration modifies the seasonal distribution of heat between the Northern and Southern hemispheres with an increase (reduction) of thermal seasonality in the Northern (Southern) Hemisphere. During the LGM, changes in boundaries conditions pertain mainly to reduced concentrations of greenhouse gases (Table 2), lower sea level and the presence of large continental ice-sheets, while the orbital configuration was similar to the pre-industrial period. Presented differently, the mid-Holocene set of simulations is useful to quantify the response of GCMs to changes in the orbital configuration while the LGM boundary conditions reflect the impact of a strong reduction in the atmospheric concentration in greenhouse gases, the presence of large continental ice sheets and lower sea level.

Table 2

Summary of the major parameters selected for each PMIP3/CMIP5 experimental design. More details can be found in (Braconnot et al., 2012; Taylor et al., 2012) and at <https://wiki.lsce.ipsl.fr/pmip3/doku.php/pmip3:design:index>.

Simulation	Orbital parameters			Trace gases				
	Eccentricity	Obliquity	Perihelion-180°	CO ₂	CH ₄	N ₂ O	CFC	O ₃
PI	0.016724	23.446°	102.04°	280 ppm	760 ppb	270 ppb	0	Modern-10 DU
6k	0.018682	24.105°	0.87°	280 ppm	650 ppb	270 ppb	0	Same as PI
21k	0.018994	22.949°	114.42°	185 ppm	350 ppb	200 ppb	0	Same as PI

Table 3

PMIP3/CMIP5 models used in this study. The last two columns indicate the name of the run when the model was used to simulate the mid-Holocene and/or the LGM. AO: coupled Atmosphere-Ocean GCMs (vegetation is prescribed to the model), AOV: coupled Atmosphere-Ocean-Vegetation GCMs (vegetation is computed by the model). In PMIP3, all the models are based on 365-days year with the vernal equinox fixed on the 21st of March at noon (Berger, 1978; Joussaume and Braconnot, 1997).

Model name	Modelling center	Type	Grid	Reference(s)	6k	21k
BCC-CSM1-1	Beijing Climate Center, China Meteorological Administration (BCC – CMA)	AOV	Atm: 128 × 64 × L26 Ocean: 360 × 232 × L40	Xin et al. (2013)	r1i1p1	
CCSM4	National Center for Atmospheric Research (NCAR), USA	AO	Atm: 288 × 192 × L26 Ocean: 320 × 384 × L60	Gent et al. (2011)	r1i1p1 r2i1p1	r1i1p1 r2i1p1
CNRM-CM5	Centre National de la Recherche Météorologique (CNRM) & Centre Européen de Recherche et de Formation Avancées en Calcul Scientifique (CERFACS), France	AO	Atm: 256 × 128 × L31 Ocean: 362 × 292 × L42	Voldoire et al. (2012)	r1i1p1	r1i1p1
COSMOS-ASO	Alfred Wegener Institute, Helmholtz Centre for Polar and Marine Research	AOV	Atm: 96 × 48 × L19 Ocean: 120 × 101 × L40	Jungclaus et al. (2006), Raddatz et al. (2007) and Roeckner et al. (2003)	r1i1p1	
CSIRO-MK3-6-0	Queensland Climate Change Centre of Excellence (QCCCE), Australia	AO	Atm: 92 × 96 × L18 Ocean: 192 × 192 × L31	Jeffrey et al. (2013) Rotstayn et al. (2012)	r1i1p1	
CSIRO-MK3L-1-2	University of New South Wales, Australia	AO	Atm: 64 × 56 × L18 Ocean: 128 × 112 × L21	Phipps et al. (2011, 2012)	r1i1p1	
FGOALS-G2	Institute of Atmospheric Physics, Chinese Academy of Sciences (LASG-IAP)	AOV	Atm: 128 × 60 × L26 Ocean: 360 × 180 × L30	Li et al. (2013)	r1i1p1	r1i1p1
FGOALS-S2	Institute of Atmospheric Physics, Chinese Academy of Sciences (LASG-IAP)	AOV	Atm: 128 × 60 × L26 Ocean: 360 × 180 × L30	Bao et al. (2013)	r1i1p1	
GISS-E2-R	Goddard Institute for Space Studies (GISS), USA	AO	Atm: 144 × 90 × L40 Ocean: 288 × 180 × L32	Schmidt et al. (2014a,b)	r1i1p1	r1i1p150 r1i1p151
IPSL-CM5A-LR	Institut Pierre Simon Laplace (IPSL), France	AOV	Atm: 96 × 96 × L39 Ocean: 182 × 149 × L31	Dufresne et al. (2013)	r1i1p1	r1i1p1
MIROC-ESM	Japan Agency for Marine-Earth Science and Technology, Atmosphere and Ocean Research Institute (The University of Tokyo), and National Institute for Environmental Studies	AOV	Atm: 128 × 64 × L80 Ocean: 256 × 192 × L44	Sueyoshi et al. (2013) Watanabe et al. (2011)	r1i1p1	r1i1p1
MPI-ESM-P	Max Planck Institute für Meteorologie (MPI), Germany	AO	Atm: 196 × 98 × L47 Ocean: 256 × 220 × L40	Giorgetta et al. (2013)	r1i1p1 r1i1p2	r1i1p1 r1i1p2
MRI-CGCM3	Meteorological Research Institute (MRI), Japan	AO	Atm: 20 × 160 × L48 Ocean: 364 × 368 × L51	Yukimoto et al. (2012)	r1i1p1	r1i1p1

Data from 13 different models (15 different runs, Table 3) were obtained from the PMIP3/CMIP5 database in March 2015 (<http://esgf-node.ipsl.fr/esgf-web-fe>, Taylor et al., 2012). When two different runs were available for one model (CCSM4 for the mid-Holocene; CCSM4 and GISS-E2-R for the LGM), data were averaged to produce one output per model to avoid overweighting any single model (Hargreaves et al., 2013). For the purpose of this study, ensemble models were calculated after interpolating each model on a 1° × 1° grid with the software CDO (CLimate Data Operators,

Schulzweida et al., 2014).

2.2. Palaeorecords selection

We have compiled a subset of records that are generally considered to reflect changes in local/regional rainfall amount and/or intensity (Table 1, Fig. 1A). This strict criterion restricts the depth of our dataset selection, as the majority of records from Africa are in fact proxies of aridity, i.e. they measure the past environmental

water-balance (precipitation minus evapotranspiration (P-PET)). Aridity is a composite variable that integrates different aspects of climate such as rainfall and temperature, as well as their seasonality. Aridity records cannot be interpreted directly in terms of rainfall without being at least corrected for the negative and non-linear effect of temperature (Chevalier and Chase, 2016). To increase the statistical power of our analysis, we nonetheless selected some aridity records (lake-levels, XRF counts and surface runoff proxies; Table 1), but only when they were indicating, at least broadly, increased/decreased rainfall signals that contrasted with predicted signals if PET was a dominant control (cf. the lake level records of our compilation, Table 1). When the interpretation was unclear, the record was excluded to reduce potential sources of error.

We used two types of rainfall proxies amount/intensity proxies: 1) isotopic proxies such as $\delta^{18}\text{O}$, measured from speleothems (McDermott, 2004; Partin et al., 2008; Shakun et al., 2007; Wang et al., 2001), or δD , measured on long-chain monocarboxylic fatty acids in lacustrine or marine sediments (Feakins and Sessions, 2010; Hou et al., 2008; Schefuß et al., 2005; Tierney et al., 2011b) and 2) quantified pollen-based reconstructions using the CREST climate reconstruction method (Chevalier et al., 2014). It is worth mentioning that regional δD records are usually interpreted as reflecting changes in rainfall amount and/or intensity. However, it has been recently pointed out that other factors, such as changes in the moisture source, could significantly impact the nature of the signal (Konecky et al., 2011; Tierney et al., 2011a). Considering the context, nature and resolution of this study, these additional factors are unlikely to significantly impact the results. Finally, since the two δD records from of the Zambezi River mouth are derived from two nearby (<65 km) marines cores (Schefuß et al., 2011; Wang et al., 2013), and share very similar trends for their overlapping section (0–17 ka), we only used one of them for each experiment to exclude any form of redundancy: the higher-resolution record of Schefuß et al. (2011) for the mid-Holocene experiment and the longer record of Wang et al. (2013) for the LGM experiment.

Following standard protocol (e.g. Bartlein et al., 2011), we chose the periods 5.5–6.5 cal kBP and 20–22 cal kBP to represent the mid-Holocene and the LGM respectively. Anomalies were calculated by subtracting the average of the last millennium. The latter criterion excludes some of the longest and best-dated sequences from which the last millennium is missing such as the δD records from lakes Victoria (Berke et al., 2012), Tanganyika (Tierney et al., 2008) and Tana (Costa et al., 2014). For the latter, however, strong similarities are observed with a Ti XRF counts record from the same lake between 1.5 and 15 cal kBP (Marshall et al., 2011). Hence, even if that proxy generally reflects aridity, we assume here that it can be interpreted as a proxy for rainfall amount/intensity in this situation. Our dataset is finally composed of 16 and 11 data points for the mid-Holocene and the LGM, respectively. Some studies have used longer time windows to include more records (e.g. Di Nezio and Tierney, 2013), but our approach prevents including additional sources of climate variability that are not incorporated in PMIP3 simulations.

In conclusion, limitations of this data compilation are: 1) the number of records, especially for the LGM, 2) the heterogeneous nature of those records and 3) the qualitative nature of the majority of them. Hence, statistically significant maps cannot be derived, limiting our study to an analysis of the broadest climate trends simulated by the models supported by point-based comparisons.

2.3. Model's evaluation

To measure the agreement between models and palaeorecords, qualitative comparisons (i.e. comparisons of the sign of the

anomalies) were performed between the proxy value and the simulated rainfall. For the marine records (records 3 and 12) and the two multi-sites stacks from southern Africa (records 15 and 16), we averaged all the values within their attraction basin (represented in green on Fig. 1A). For the other records, we performed point-based comparisons. We used the kappa statistic (κ) to measure the global agreement between the simulations and the palaeodata. This statistic is based on the comparison of the categorical classification performed by two independent 'raters' (namely here, the models and the data) (Cohen, 1960). It varies between -1 (models and data are never showing the same anomaly) and 1 (perfect agreement, i.e. models and data always predict the same anomaly sign). The kappa statistics also integrates the notion of random agreement (false positive, $\kappa=0$). We defined three categorical levels for our rainfall anomalies: wetter, drier and no change. Palaeo-data were sorted in the 'no change' category when the average of the 6k/21k time window was not statistically different at 95% (Student t-test) from the average of the last millennium (Table 1). To define the 'no change' category for models, we kept some flexibility and rather used a moving threshold from 0 to 0.5 mm/day that we moved with a 0.01 mm/day step. We refer to Di Nezio and Tierney (2013) for further details about the application of this index.

3. Results

3.1. Definition of the rainy season

Simulations of the PI rainfall in southeastern and northeastern Africa (as defined with the boxes on Fig. 1B) are consistent, both in terms of amplitude and seasonality (Fig. 2 Top), with the modern climatology of Worldclim (Hijmans et al., 2005). However, we do observe an inversion of the two rainfall peaks in eastern-equatorial Africa with the first maximum occurring in November instead of April, and the second peak in May instead of November. Interestingly, and despite that inversion, cumulated rainfall amounts for the overall rainy season remains fairly consistent between models and modern climatology. To define our rainfall season, we thus had to select a period that is long enough to include these two peaks, but also short enough to exclude the influence of temperate systems during the winter months in southeastern Africa (Fig. 1C). In addition, as our study area covers a large latitudinal extent (20°N – 30°S), we had to consider that the rainfall maximum occurs at different times of the year (Fig. 1C). To represent the regionally specific period of maximum rainfall, we derived a variable that represents the five consecutive months with the highest cumulative rainfall amounts (PWet5M, Fig. 1C). This choice of five months reflects a trade-off between the different constraints aforementioned.

3.2. Mid-Holocene

In the ensemble simulation, an axis parallel to the Equator at ~3–5°S divides our study area in two, with higher PWet5M values being simulated to the north (from Lake Victoria and northward) and lower to the south (Lakes Tanganyika and Malawi, southeastern Africa and Madagascar, Fig. 3). Inter-model agreement is high north of the Equator and south of 10°S (red dots and crosses on Fig. 3), but differences are notable in the transition area that encompasses the latitudes of Lakes Victoria and Tanganyika (0–10°S). This north/south rainfall dipole is consistent among model simulations with most of the variability being explained by 1) latitudinal shifts of that transition zone and 2) the amplitude of the anomaly simulated over the Ethiopian highlands and the northwestern Indian Ocean (Fig. 3).

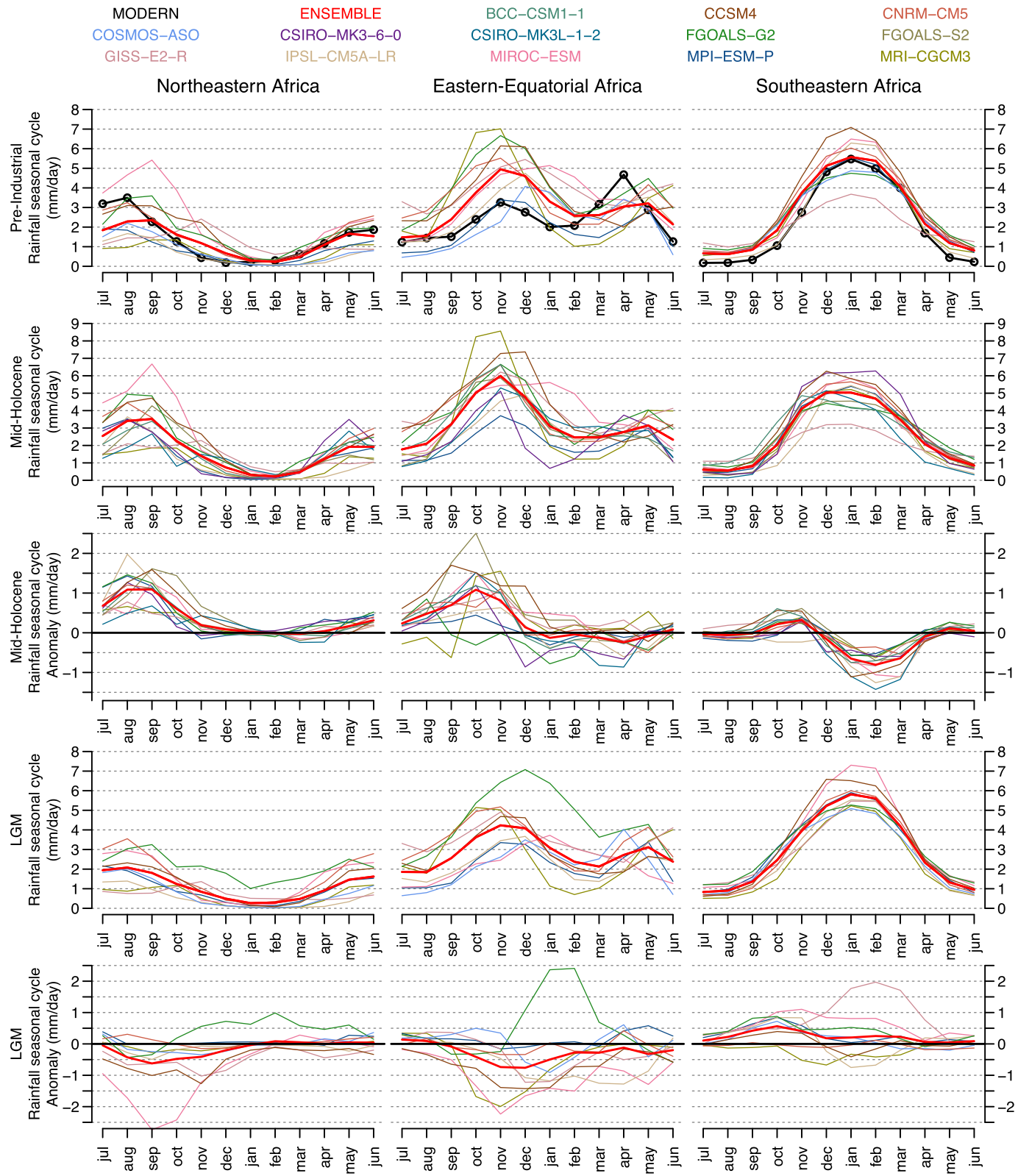


Fig. 2. Mid-Holocene and LGM rainfall annual cycle (mm.d^{-1}) for northeastern, eastern-equatorial and southeastern Africa (as defined by the boxes on Fig. 1). Red thick lines represent the ensemble models. Modern values, extracted from Worclim 1.4 database (Hijmans et al., 2005), are indicated in black with black open circles. (For interpretation of the references to colour in this figure legend, the reader is referred to the web version of this article.)

The distribution of anomalies from the palaeodata follows a similar spatial pattern (Fig. 3). Interestingly, it is also in this

transition region ($0\text{--}10^\circ\text{S}$) that two palaeo-datasets exhibited non-significant rainfall anomalies (Table 1; Bonnefille and Chalié, 2000;

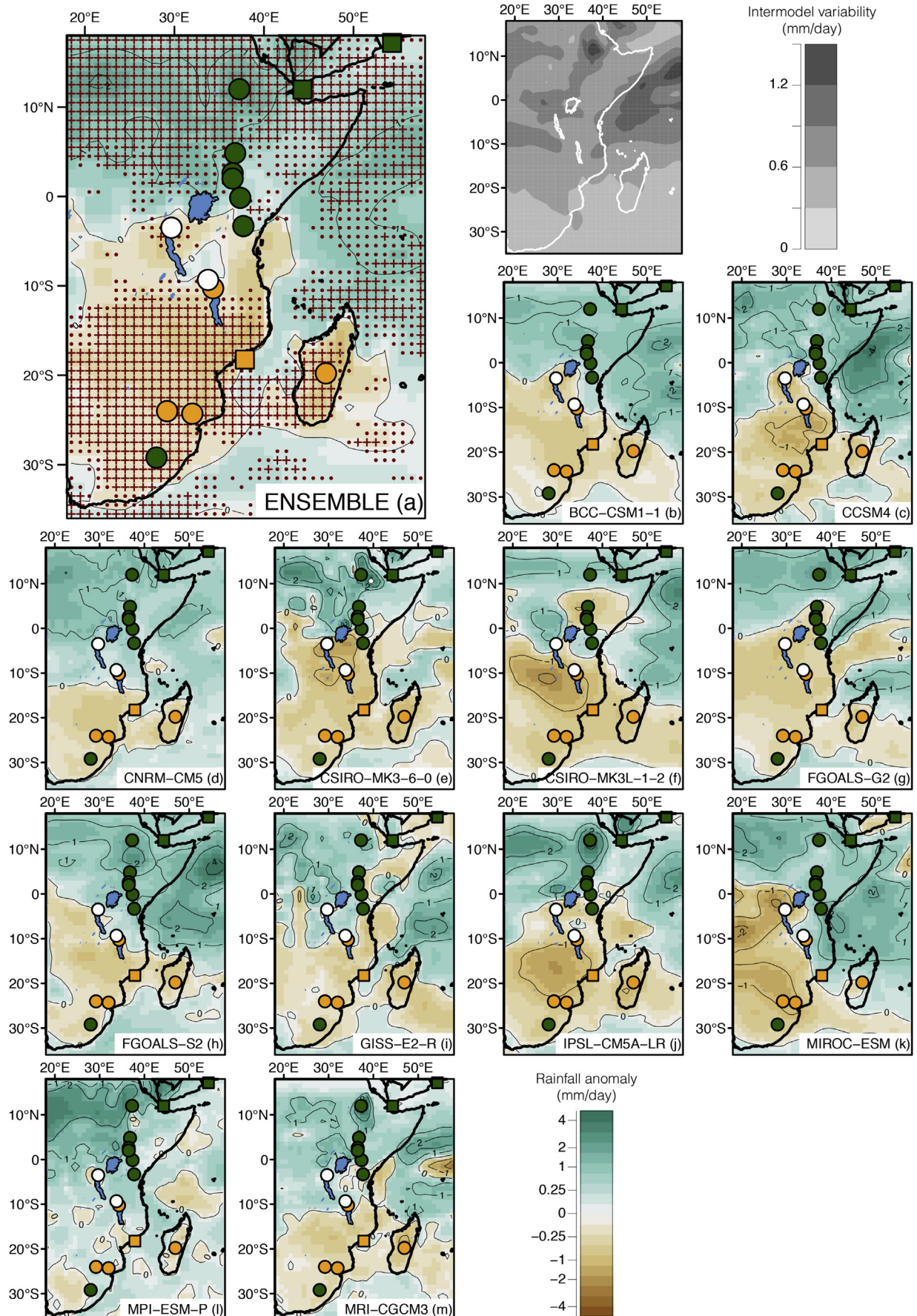


Fig. 3. Mid-Holocene PWet5M anomaly maps as simulated by PMIP3 models. Green/White/Orange dots (squared for marine cores and rounded for terrestrial records) indicate positive/not significant/negative rainfall anomalies as inferred from the palaeodata. The brown to green rainfall colour scale represents the simulated rainfall anomalies. Note that the colour scale is not linear. Inter-model agreement on the sign of the anomalies at ~75/90%, which correspond to an agreement of 9 and 11 out of the 12 models, is indicated by red dots/crosses, respectively. The top right grey map represents the inter-model variability, calculated as the standard deviation of the model values, for PWet5M during the mid-Holocene. The darker the grid cell is, the more divergent the models are. (For interpretation of the references to colour in this figure legend, the reader is referred to the web version of this article.)

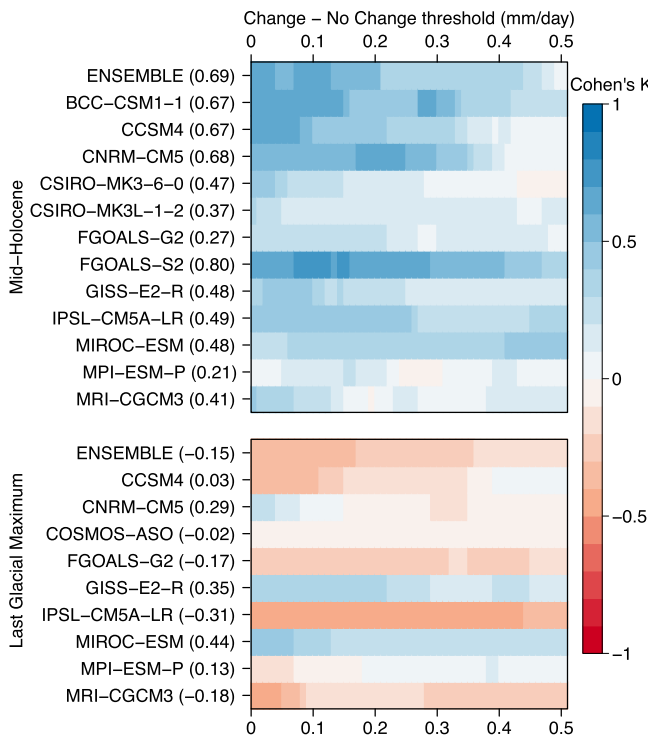


Fig. 4. Kappa statistics calculated for each model and each period. The x-axis represents the varying threshold used to define the “no change” rainfall anomalies (from 0 to 0.5 mm/day). The highest kappa found for each model is indicated between parentheses. The darker the blue/red shading is, the better/worse the data-model agreement is. (For interpretation of the references to colour in this figure legend, the reader is referred to the web version of this article.)

(Garcin et al., 2006), indicating similar mid-Holocene and last millennium conditions. Based on the kappa statistics, models that perform best are the ensemble ($\kappa=0.69$, Fig. 4), BCC-CSM1-1 (0.67), CCSM4 (0.67), CNRM-CM5 (0.68) and FGOALS-s2 (0.80). With their small kappa statistics, MPI-ESM-P ($\kappa=0.21$) and FGOALS-G2 (0.27) have a very low predictive capacity. FGOALS-G2 simulates a north-south rainfall dipole, but the transition zone is located too far north, explaining its low kappa. On the contrary, MPI-ESM-P simulates increased rainfall across almost all of the study area with the exception of spatially restricted patches of negative anomalies.

In northeastern and eastern-equatorial Africa, the annual amount of rainfall increases significantly (+0.5 to +1 mm.d⁻¹, Fig. 2) during the wettest period, i.e. from May to October for the former and from July to November for the latter. Seasonal cycles remain unchanged as these changes already correspond to the most important peak of rainfall. In eastern-equatorial Africa, a small decrease is observed at the time of the second peak (-0.2 mm.d⁻¹). In southeastern Africa, the pattern of rainfall anomalies is similar in that rainfall monthly means increase slightly from October to November (+0.2 mm.d⁻¹) and decrease from December to April (less summer rain -0.7 mm.d⁻¹), but the gain does not compensate for the loss, resulting in an overall loss of precipitation.

3.3. Last Glacial Maximum

Compared to the 6k experiment, an inverse north-south negative/positive rainfall anomaly dipole is visible in the ensemble model of the 21k experiment, with a limit situated at ~15°S, along the modern southernmost position of the ITCZ (Fig. 5). However, this averaged representation masks strong inter-model variability, both in terms of spatial distribution and amplitude of change.

While broadly similar spatial patterns are visible in many simulations, such as the aridification of northeastern Africa and parts of eastern-equatorial Africa, or the humidification of the lower Zambezi basin (cf. the red dots and crosses on the ensemble model, Fig. 5), strong divergence occurs in coastal and high altitude regions. Looking more specifically, we can distinguish that each model is, in fact, simulating a unique synoptic pattern of rainfall anomalies, none of which reflecting the pattern suggested by the palaeo-data. Models identified in the previous section with a good predictive capacity (CCSM4 and CNRM-5) are not distinguished here, and their agreement with the spatial distribution of palaeodata is indistinguishable from random agreement ($\kappa \sim 0$, Fig. 4).

Despite being spatially divergent, trends in seasonal changes observed in the ensemble model are fairly homogeneous when averaged by region. Northeastern Africa experiences reduced rainfall intensity from July to December (-0.7 mm.d⁻¹ during the peak month). A wetter, symmetrical climate evolution is observed during the same period in southeastern Africa. Eastern equatorial Africa experiences drier months year-round, with the largest decrease being observed at the time of the dominant rainfall peak (-0.8 mm.d⁻¹ in November and December). Those changes result in a shorter/longer rainy season in northeastern and southeastern Africa, respectively, while the difference between the two rainfall maxima characteristic of eastern equatorial African climate during the pre-industrial and mid-Holocene periods is less marked.

4. Discussion

4.1. Mid-Holocene

All mid-Holocene model outputs analysed are in good agreement with mid-Holocene palaeodata, indicating negative rainfall anomalies south of 3–5°S and positive anomalies northward (Figs. 3 and 4). The two non-significant rainfall anomalies inferred from the palaeo-data (Table 1) are consistent with the small anomalies simulated in the transitional band defined by the southernmost and northernmost latitudes of lakes Tanganyika and Victoria, respectively. This continental-scale pattern of rainfall anomalies suggests an intensified northern monsoon from May to November, and a weaker southern monsoon from December to April (Fig. 5B), a dynamic that can be directly linked to variations in the amount of heat received by the tropics (Fig. 7 Top). The orbital configuration at 6 ka promotes an increased/reduced seasonal heating in the Northern/Southern Hemisphere, so that summer is warmer in the Northern Hemisphere and colder in the Southern Hemisphere, and vice-versa in winter. This configuration allows the northern monsoon to intensify and expand (Fig. 6B) as stronger seasonal thermal amplitude results in stronger thermal land-sea contrasts, deeper low-pressure cells over land, and therefore enhanced advection of moist air from the Indian and Atlantic oceans. An inverse dynamic occurred in southeastern Africa, where the strength of the southern monsoonal systems weakened. However, simulations suggest that the strongest reduction of summer rainfall occurs mainly on the margins of the southern monsoon core, located over Zambia (Fig. 6B).

This north/south opposition is consistent with the rainfall dipole of the AHP, which has often been explained by a migration of the ITCZ further north during the boreal summer in response to the warming of the Northern Hemisphere (Braconnot et al., 2007b, 2000; Coe and Harrison, 2002; deMenocal et al., 2000; Kutzbach, 1981; Prell and Kutzbach, 1987). PMIP3 models rather suggest that the positive rainfall anomalies are caused by an overall intensification of the monsoon domain north- and southward that eventually brings more rainfall across northern, and part of tropical Africa. The opposite is simulated during the austral summer with a

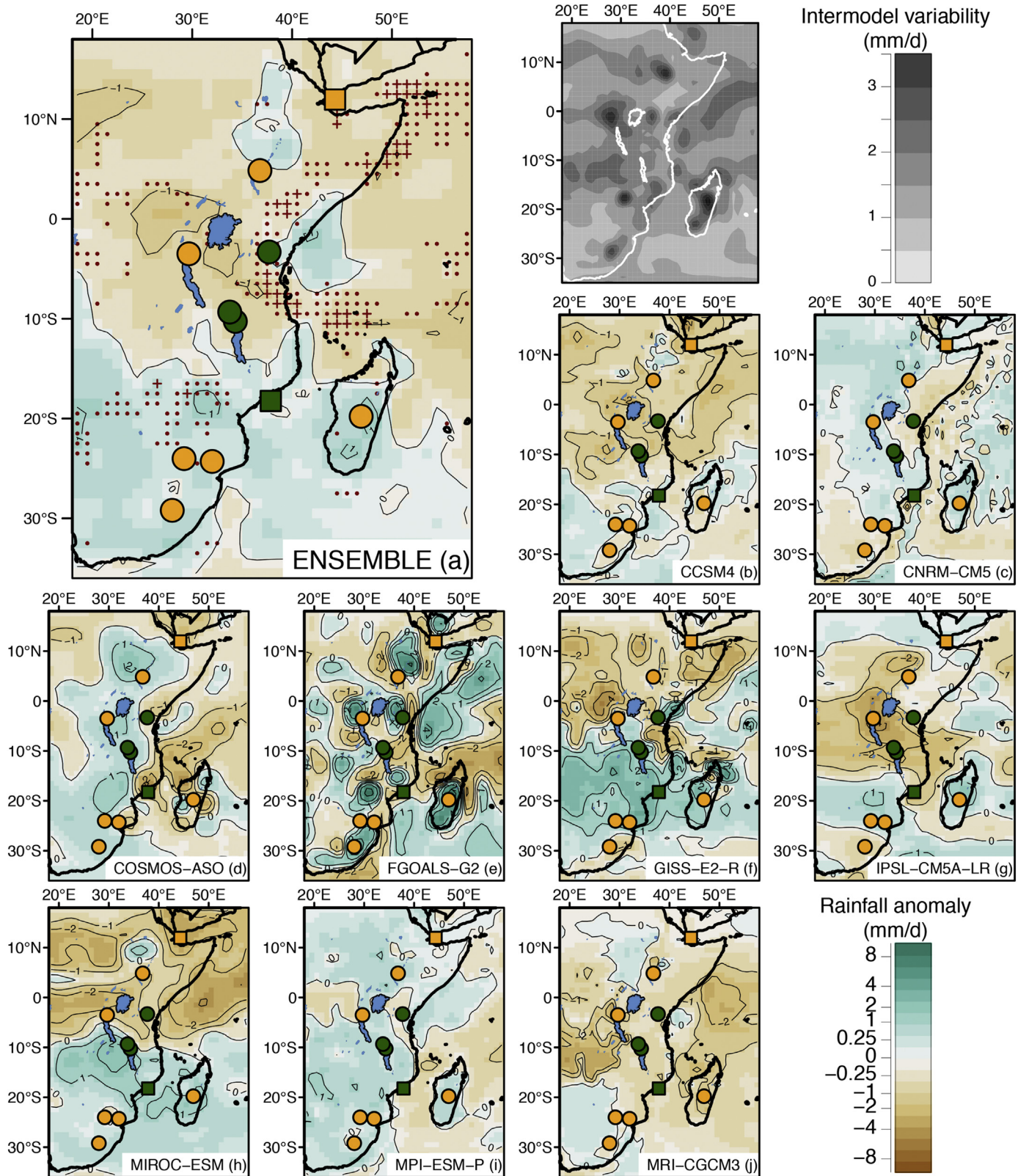


Fig. 5. LGM PWet5M anomaly maps as simulated by PMIP3 models. Green/White/Orange dots (squared for marine cores and rounded for terrestrial records) indicate positive/not significant/negative rainfall anomalies as inferred by the palaeodata. The brown to green rainfall colour scale represents the simulated rainfall anomalies. Note that the colour scale is not linear. Inter-model agreement on the sign of the anomalies at -75/90%, which correspond to an agreement of seven and eight out of the nine models, is indicated by red dots/crosses, respectively. The top right grey map represents the inter-model variability, calculated as the standard deviation of the model values, for PWet5M during the LGM. The darker the grid cell is, the more divergent the models are. (For interpretation of the references to colour in this figure legend, the reader is referred to the web version of this article.)

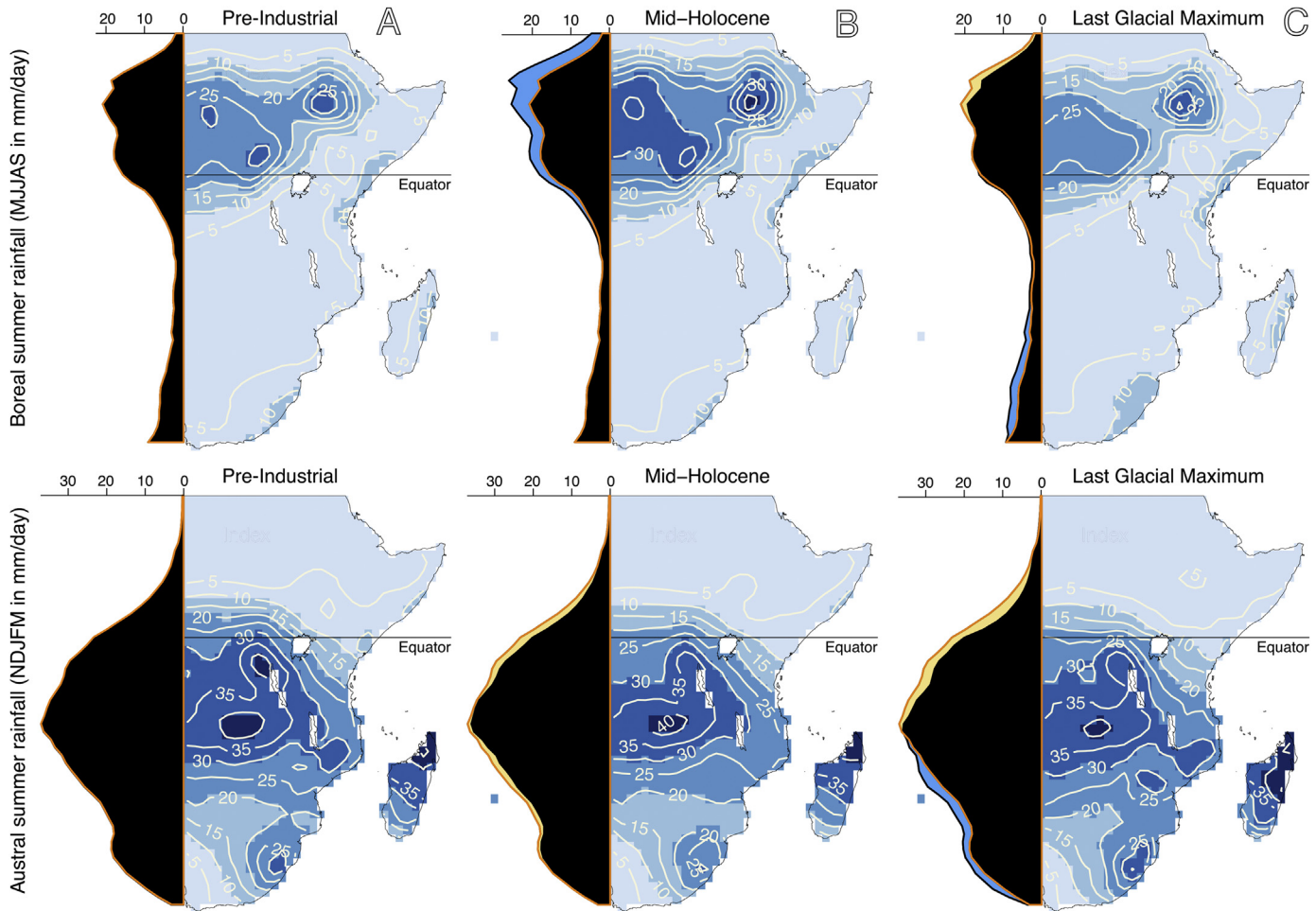


Fig. 6. (A) Representation of the simulated rainfall patterns for MJAS (boreal summer, top) and NDJFM (austral summer, bottom) during the pre-Industrial period. The black shading with an orange contour on the left side of each map represents the longitudinal average of rainfall distribution of rainfall during the pre-Industrial period. For panes B (mid-Holocene) and C (LGM), longitudinal averages are recalculated and compared to the PI values (orange contour). When the amount of rainfall is higher/lower than the PI value, the shading is represented in blue/yellow. (For interpretation of the references to colour in this figure legend, the reader is referred to the web version of this article.)

reduced intensity of the core and a contraction of the rainbelt in the equatorial region (Fig. 6B). Those observations are consistent with the results of Jiang et al. (2015a), who showed similar behaviour for all northern (expansion and intensification) and southern (contraction and weakening) monsoon domains, and linked those changes to variations of the equator-to-pole and land-sea thermal gradients driven by orbital precession.

Many studies conducted in northern Africa have shown that models underestimate the apparent amplitude of change during the AHP (Braconnot et al., 2012; Harrison et al., 2015; Perez-Sanz et al., 2014). Whether similar quantitative conclusions can be applied to our study area is still beyond the capacity imposed by the number and quality of the palaeorecords available. Records from southeastern Africa suggest the opposite, with an overestimation of the arid anomalies (Chevalier and Chase, 2015; Holmgren et al., 2003; Schefuß et al., 2011), particularly over the lower Zambezi basin (-0.5 mm/day , Fig. 3). If the sign of the rainfall anomaly is correct, the δD records from marine cores GeoB9307-3 (Schefuß et al., 2011) and GIK 16160-3 (Wang et al., 2013) indicate little difference between mid-Holocene and pre-industrial conditions, suggesting that some models may in fact overestimate the dry anomalies. Noteworthy is the decrease of those anomalies from PMIP1 to PMIP2 and from PMIP2 to PMIP3 (Jiang et al., 2015a), indicating that models are probably making significant progress in

that region for the mid-Holocene period.

4.2. Last Glacial Maximum

With low, and even negative, kappa statistics (Fig. 4), the different simulations, and the ensemble model, suggest conditions significantly different from the pattern inferred from the palaeodata (Fig. 5). Tierney et al. (2008) and Chevalier and Chase (2015) have proposed that the reduction of precipitation over most of the study area was a response to the colder atmospheric and oceanic conditions that reduced air moisture content during the LGM, with the notable exception of a restricted coastal region between the Equator and $\sim 20^\circ\text{S}$ (Di Nezio et al., 2016; Di Nezio and Tierney, 2013). While the limited number of continuous and well-dated terrestrial precipitation proxy records from the region precludes the identification of the exact extent of this wetter continental area, the eastern margin of the African Rift seems to be playing an important role in separating these positive and negative rainfall anomalies. The ensemble model – *i.e.* the model that represents the large-scale trends shared by all the models – does not capture this continental-scale pattern, indicating rather a north/south dipole with reduced/increased precipitation, respectively. This simulated dipole is the consequence of a contraction of the northern monsoon domain during the boreal summer, and of a

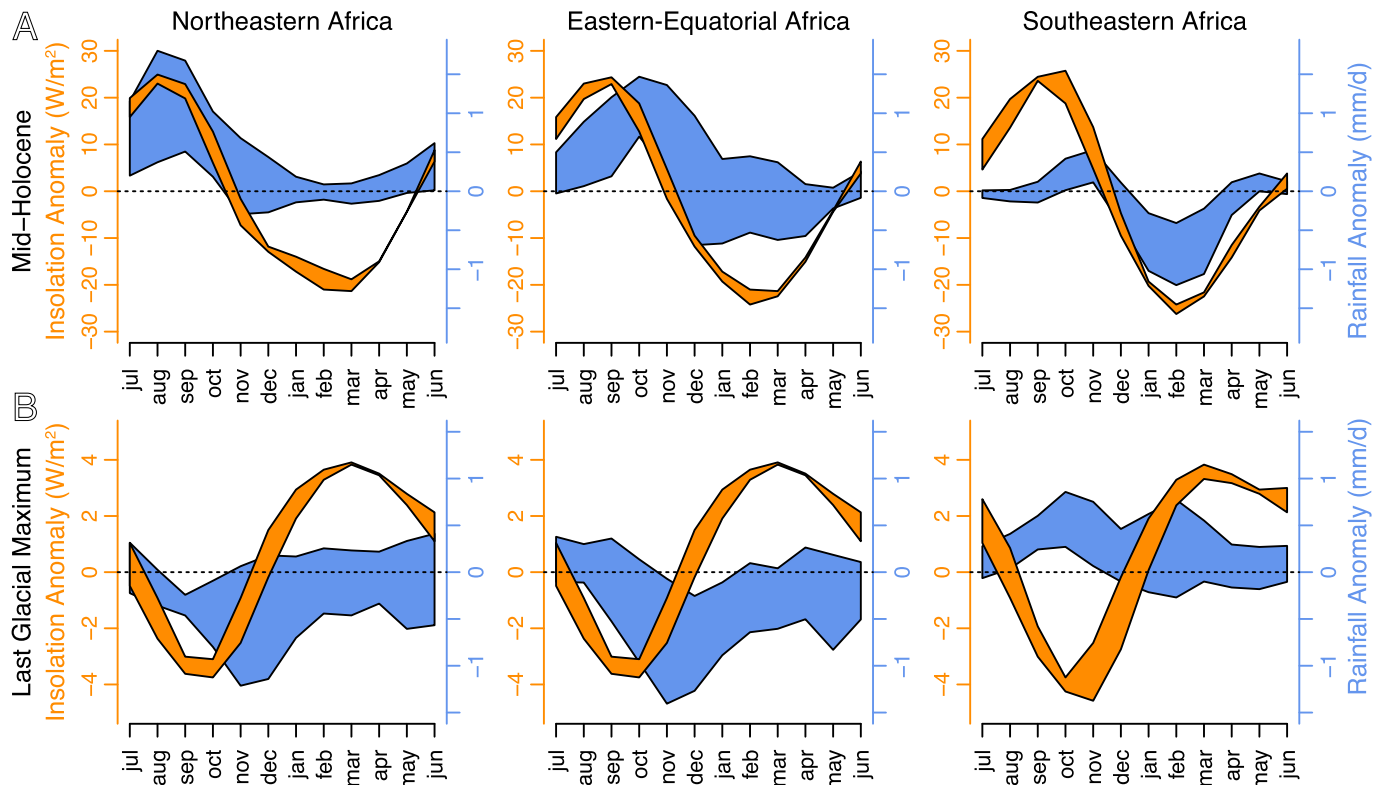


Fig. 7. Monthly rainfall anomalies from the ensemble models (blue) vs. changes in insolation (orange) for the mid-Holocene (A) and the LGM (B). Insolation and rainfall values correspond to the average plus or minus one standard deviation of all the grid cells part of the regional boxes defined on Fig. 1. (For interpretation of the references to colour in this figure legend, the reader is referred to the web version of this article.)

2–3° southward migration of the southern domain as a whole, without any significant change in its absolute latitudinal range or intensity (Fig. 6C). However, this dynamic is not a significant synoptic response as each model simulates a unique pattern for the anomaly (Fig. 5). This inter-model heterogeneity suggests rather that some fundamental mechanisms or important feedbacks underlying the LGM mean climate state and sensitivities are not captured, misattributed or not given enough importance in the models.

Two major discrepancies between the palaeo-data and the PMIP3 LGM ensemble rainfall simulations have been identified. The first one concerns the wetter conditions across southeastern Africa. The orbital configuration of the LGM being very similar to the pre-industrial period (Table 2), the small variations of insolation cannot explain these conditions (Fig. 7). The annual distribution of rainfall anomalies and changes in the seasonal cycles (Figs. 2 and 7) rather suggests that the rainbelt had a longer residence time in the Southern Hemisphere during the LGM, which is a consistent response to the cooling of the Northern Hemisphere coupled to the development of large continental ice-sheets (Arbuszewski et al., 2013; Broecker and Putnam, 2013; Clark et al., 2009). However, this change does not explain the simulated north/south rainfall dipole as monsoon intensity should be reduced by the colder continental and sea surface temperatures (Chevalier and Chase, 2015). The simulated SST reduction (1 °C in the northwestern and 2–2.5 °C in the southwestern sectors of the Indian Ocean), an amplitude of change consistent with the data (Bard et al., 1997; Dahl and Oppo, 2006; Sonzogni et al., 1998), should significantly reduce moisture content of the tropical easterlies and ultimately reduce the latitudinal range of the southern monsoon domain relative to PI (Chevalier and Chase, 2015; Jiang et al., 2015a, 2015b).

The second feature not captured by models is the apparently wetter coastal band between the Equator and 20°S. This patch of positive rainfall anomalies has been linked to changes in the strength of the zonal atmospheric circulation over the Indian Ocean basin as a response to the LGM lower sea-level (Di Nezio et al., 2016; Di Nezio and Tierney, 2013). The exposure of the Sunda and Sahul shelves in the middle of the Indo-Pacific Warm Pool (90–150°E, 20°S–20°N) increased the regional albedo, which initiated a reduction in convection that eventually resulted, via a positive feedback of the Indian Ocean circulation, in an augmentation of the East-West SST gradient and a weakening of the entire Indian Ocean Walker Cell (Di Nezio et al., 2016). Reduced subsidence in the western/descending branch of the cell resulted in a positive rainfall anomaly over the western Indian Ocean basin and easternmost Equatorial Africa (Hastenrath, 2001, 2000; Nicholson, 2015). Di Nezio and Tierney (2013) have already showed from a subset of PMIP2 and PMIP3 models that this large-scale mechanism of the LGM was absent in the simulations, and this study extends their results and conclusions to all the PMIP3 model simulations for this region.

5. Conclusion

The publication of new palaeodata from a large region covering the Horn of Africa to southeastern Africa has significantly improved the potential for large-scale data/model comparison in that region. In this study, the mid-Holocene and Last Glacial Maximum precipitation simulations were investigated using the results of PMIP3/CMIP5 experiments. For the mid-Holocene, the response is reasonably robust and homogenous among all model tested. Models are sensitive to changes in the distribution of heat between

the Northern and Southern hemispheres and reproduce the more humid/arid north/south dipole that is characteristic of the end of the African Humid Period. Simulations of the LGM are far less consistent and inter-model variability is high. Each model simulates a unique pattern of precipitation anomalies, none of which being able to capture the signal evident in the palaeo-data. Two major discrepancies have been identified in the LGM simulations:

1. In contrast with the palaeo-data, models simulate more precipitation across southeastern Africa as a response to a longer residence time of the tropical rainbelt in the Southern Hemisphere, and more critically to a limited sensitivity of the southern African monsoon to the 2–2.5 °C colder SSTs of the southwestern Indian Ocean.
2. Models fail to capture the variability of the Indian Ocean Walker Cell, whose intensity decreased during the LGM because of the exposure of the Sahul and Sunda shelves. Reduction of this zonal circulation ultimately led to increase precipitation over the western sector of the Indian Ocean and easternmost equatorial Africa.

This study highlights that the parameterization of tropical climate in GCMs is still incomplete. To improve model simulations, a major focus should be held on integrating these atmospheric and oceanic teleconnections that exist between the different interconnected monsoon domains of the Global Monsoon. The dynamic of the Indian Ocean Walker circulation that links the African and Southeast Asian monsoon domains is not captured in any PMIP3 models, which could explain the lack of consistency between the simulations.

Acknowledgments

Funding was received from the European Research Council (ERC) under the European Union's Seventh Framework Programme (FP7/2007–2013)/ERC Starting Grant "HYRAX", grant agreement no. 258657. The NCEP Reanalysis Derived data and NOAA_OI_SST_V2 data are provided by the NOAA/OAR/ESRL PSD, Boulder, Colorado, USA, from their web site at <http://www.esrl.noaa.gov/>. This is an ISEM publication number 2016-255.

References

- Amante, C., Eakins, B.W., 2009. Etopo1 1 Arc-minute Global Relief Model: Procedures, Data Sources and Analysis. NOAA Tech. Memo. NESDIS NGDC-24. Natl. Geophys. Data Center, NOAA.
- Anderson, P.M., Barnosky, C.W., Bartlein, P.J., Behling, P.J., Brubaker, L., Cushing, E.J., Dodson, J., Dworaksky, B., Guetter, P.J., Harrison, S.P., Huntley, B., Kutzbach, J.E., Markgraf, V., Marvel, R., McGlone, M.S., Mix, A.C., Moar, T., Morley, J., Perrott, R.A., Peterson, G.M., Prell, W.L., Prentice, I.C., Ritchie, J.C., Roberts, N., Ruddiman, W.F., Salinger, M.J., Spaulding, W.G., Street-Perrott, F.A., Thompson, R.S., Wang, P.K., Webb, T.I., Winkler, M.G., Wright, H.E.J., 1988. Climatic changes of the last 18,000 years: observations and model simulations. *Science* (80–) 241 (4869), 1043–1052.
- Annan, J.D., Hargreaves, J.C., 2010. Reliability of the CMIP3 ensemble. *Geophys. Res. Lett.* 37, L02703.
- Annan, J.D., Hargreaves, J.C., 2011. Understanding the CMIP3 multimodel ensemble. *J. Clim.* 24, 4529–4538.
- Arbuszewski, J.A., DeMenocal, P.B., Cléroux, C., Bradtmiller, L., Mix, A.C., 2013. Meridional shifts of the Atlantic intertropical convergence zone since the last glacial maximum. *Nat. Geosci.* 6, 959–962.
- Baker, A., Routh, J., Blaauw, M., Roychoudhury, A.N., 2014. Geochemical records of palaeoenvironmental controls on peat forming processes in the Mfabeti peatland, Kwazulu Natal, South Africa since the Late Pleistocene. *Palaeogeogr. Palaeoclimatol. Palaeoecol.* 395, 95–106.
- Bao, Q., Lin, P., Zhou, T., Liu, Y., Yu, Y., Wu, G., He, B., He, J., Li, L., Li, J., Li, Y., Liu, H., Qiao, F., Song, Z., Wang, B., Wang, J., Wang, P., Wang, X., Wang, Z., Wu, B., Wu, T., Xu, Y., Yu, H., Zhao, W., Zheng, W., Zhou, L., 2013. The flexible global ocean-atmosphere-land system model, spectral version 2: FGOALS-s2. *Adv. Atmos. Sci.* 30, 561–576.
- Bard, E., Rostek, F., Sonzogni, C., 1997. Interhemispheric synchrony of the last deglaciation inferred from alkenone palaeothermometry. *Nature* 385, 707–710.
- Barker, P.A., Gasse, F., 2003. New evidence for a reduced water balance in East Africa during the Last Glacial Maximum: implication for model-data comparison. *Quat. Sci. Rev.* 22, 823–837.
- Barker, P.A., Street-Perrott, F.A., Leng, M.J., Greenwood, P.B., Swain, D.L., Perrott, R.A., Telford, R.J., Ficken, K.J., 2001. A 14,000-year oxygen isotope record from diatom silica in two alpine lakes on Mt. Kenya. *Science* (80–) 292, 2307–2310.
- Bartlein, P.J., Harrison, S.P., Brewer, S., Connor, S., Davis, B.A.S., Gajewski, K., Guiot, J., Harrison-Prentice, T.L., Henderson, A., Peyron, O., Prentice, I.C., Scholze, M., Seppä, H., Shuman, B.N., Sugita, S., Thompson, R.S., Viala, A.E., Williams, J., Wu, H., 2011. Pollen-based continental climate reconstructions at 6 and 21 ka: a global synthesis. *Clim. Dyn.* 37, 775–802.
- Berger, A.L., 1978. Long-Term variations of daily insolation and quaternary climatic changes. *J. Atmos. Sci.* 35, 2362–2367.
- Berke, M.A., Johnson, T.C., Werne, J.P., Grice, K., Schouten, S., Sinnenberg Damsté, J.S., 2012. Molecular records of climate variability and vegetation response since the late Pleistocene in the lake Victoria basin, east Africa. *Quat. Sci. Rev.* 55, 59–74.
- Bonnefille, R., Chalié, F., 2000. Pollen-inferred precipitation time-series from equatorial mountains, Africa, the last 40 kyr BP. *Glob. Planet. Change* 26, 25–50.
- Bouimetarhan, I., Dupont, L.M., Kuhlmann, H., Pätzold, J., Prange, M., Schefuß, E., Zonneveld, K., 2015. Northern Hemisphere control of deglacial vegetation changes in the Rufiji uplands (Tanzania). *Clim. Past.* 11, 751–764.
- Braconnot, P., Harrison, S.P., Joussaume, S., Hewitt, C.D., Kitoh, A., Kutzbach, J.E., Liu, Z., Otto-Bliesner, B.L., Syktus, J.J., Weber, S.L., 2004. Evaluation of PMIP coupled ocean-atmosphere simulations of the Mid-Holocene. In: Battarbee, R.W., Gasse, F., Stickley, C.E. (Eds.), *Past Climate Variability through Europe and Africa, Developments in Paleoenvironmental Research*. Springer, Netherlands, Dordrecht, pp. 515–529.
- Braconnot, P., Harrison, S.P., Kageyama, M., Bartlein, P.J., Masson-Delmotte, V., Abe-Ouchi, A., Otto-Bliesner, B.L., Zhao, Y., 2012. Evaluation of climate models using palaeoclimatic data. *Nat. Clim. Chang.* 2, 417–424.
- Braconnot, P., Joussaume, S., De Noblet, N., Ramstein, G., 2000. Mid-Holocene and last glacial maximum African monsoon changes as simulated within the paleoclimate modelling intercomparison project. *Glob. Planet. Change* 26, 51–66.
- Braconnot, P., Otto-Bliesner, B.L., Harrison, S.P., Joussaume, S., Peterschmitt, J., Abe-Ouchi, A., Crucifix, M., Driesschaert, E., Fichefet, T., Hewitt, C.D., Kageyama, M., Kitoh, A., Laîné, A., Loutre, M.-F., Marti, O., Merkel, U., Ramstein, G., Valdes, P., Weber, S.L., Yu, Y., Zhao, Y., 2007a. Results of PMIP2 coupled simulations of the Mid-Holocene and Last Glacial Maximum – Part 1: experiments and large-scale features. *Clim. Past.* 3, 261–277.
- Braconnot, P., Otto-Bliesner, B.L., Harrison, S.P., Joussaume, S., Peterschmitt, J., Abe-Ouchi, A., Crucifix, M., Driesschaert, E., Fichefet, T., Hewitt, C.D., Kageyama, M., Kitoh, A., Loutre, M.-F., Marti, O., Merkel, U., Ramstein, G., Valdes, P., Weber, L., Yu, Y., Zhao, Y., 2007b. Results of PMIP2 coupled simulations of the Mid-Holocene and Last Glacial Maximum – Part 2: feedbacks with emphasis on the location of the ITCZ and mid- and high latitudes heat budget. *Clim. Past.* 3, 279–296.
- Broecker, W.S., Putnam, A.E., 2013. Hydrologic impacts of past shifts of Earth's thermal equator offer insight into those to be produced by fossil fuel CO₂. *Proc. Natl. Acad. Sci.* 110, 16710–16715.
- Burrough, S.L., Thomas, D.S.G., 2013. Central southern Africa at the time of the African Humid Period: a new analysis of Holocene palaeoenvironmental and palaeoclimate data. *Quat. Sci. Rev.* 80, 29–46.
- Castañeda, I.S., Werne, J.P., Johnson, T.C., 2007. Wet and arid phases in the southeast African tropics since the last glacial maximum. *Geology* 35, 823–826.
- Chase, B.M., Boom, A., Carr, A.S., Carré, M., Chevalier, M., Meadows, M.E., Pedro, J.B., Stager, J.C., Reimer, P.J., 2015a. Evolving southwest African response to abrupt deglacial North Atlantic climate change events. *Quat. Sci. Rev.* 121, 132–136.
- Chase, B.M., Boom, A., Carr, A.S., Meadows, M.E., Reimer, P.J., 2013. Holocene climate change in southernmost South Africa: rock hyrax midden record shifts in the southern Westerlies. *Quat. Sci. Rev.* 82, 199–205.
- Chase, B.M., Lim, S., Chevalier, M., Boom, A., Carr, A.S., Meadows, M.E., Reimer, P.J., 2015b. Influence of tropical easterlies in the southwestern Cape of Africa during the Holocene. *Quat. Sci. Rev.* 107, 138–148.
- Chase, B.M., Meadows, M.E., 2007. Late Quaternary dynamics of southern Africa's winter rainfall zone. *Earth Sci. Rev.* 84, 103–138.
- Chase, B.M., Meadows, M.E., Carr, A.S., Reimer, P.J., 2010. Evidence for progressive Holocene aridification in southern Africa recorded in Namibian hyrax middens: implications for African monsoon dynamics and the "African humid period.". *Quat. Res.* 74, 36–45.
- Chase, B.M., Meadows, M.E., Scott, L., Thomas, D.S.G., Marais, E., Sealy, J.C., Reimer, P.J., 2009. A record of rapid Holocene climate change preserved in hyrax middens from southwestern Africa. *Geology* 37, 703–706.
- Chevalier, M., Chase, B.M., 2015. Southeast African records reveal a coherent shift from high- to low-latitude forcing mechanisms along the east African margin across last glacial–interglacial transition. *Quat. Sci. Rev.* 125, 117–130.
- Chevalier, M., Chase, B.M., 2016. Determining the drivers of long-term aridity variability: a southern African case study. *J. Quat. Sci.* 31, 143–151.
- Chevalier, M., Cheddadi, R., Chase, B.M., 2014. CREST (Climate REconstruction Software): a probability density function (PDF)-based quantitative climate reconstruction method. *Clim. Past.* 10, 2081–2098.
- Clark, P.U., Dyke, A.S., Shakun, J.D., Carlson, A.E., Clark, J., Wohlfarth, B., Mitrovica, J.X., Hostettler, S.W., McCabe, A.M., 2009. The last glacial maximum. *Science* (80–) 325, 710–714.
- Claussen, M., Bathiany, S., Brovkin, V., Kleinen, T., 2013. Simulated climate-

- vegetation interaction in semi-arid regions affected by plant diversity. *Nat. Geosci.* 6, 954–958.
- Claussen, M., Brovkin, V., Ganopolski, A., Kubatzki, C., Petoukhov, V., 2003. Climate change in Northern Africa: the past is not the future. *Clim. Chang.* 57, 99–118.
- Claussen, M., Gayler, V., 1997. The greening of the Sahara during the Mid-Holocene: results of an interactive atmosphere-biome model. *Glob. Ecol. Biogeogr. Lett.* 6, 369–377.
- Coe, M., Harrison, S.P., 2002. The water balance of northern Africa during the mid-Holocene: an evaluation of the 6 Ka BP PMIP simulations. *Clim. Dyn.* 19, 155–166.
- Cohen, J., 1960. A coefficient of agreement for nominal scales. *Educ. Psychol. Meas.* 20, 37–46.
- Costa, K., Russell, J.M., Konecky, B.L., Lamb, H.F., 2014. Isotopic reconstruction of the African humid period and Congo air boundary migration at lake Tana, Ethiopia. *Quat. Sci. Rev.* 83, 58–67.
- Dahl, K.A., Oppo, D.W., 2006. Sea surface temperature pattern reconstructions in the Arabian Sea. *Paleoceanography* 21.
- deMenocal, P.B., Ortiz, J., Guilderson, T., 2000. Abrupt onset and termination of the African Humid Period: rapid climate responses to gradual insolation forcing. *Quat. Sci. Rev.* 19, 347–361.
- Di Nezio, P.N., Tierney, J.E., 2013. The effect of sea level on glacial Indo-Pacific climate. *Nat. Geosci.* 6, 485–491.
- Di Nezio, P.N., Timmermann, A., Tierney, J.E., Jin, F.F., Otto-Bliesner, B., Rosenbloom, N., Mapes, B., Neale, R., Ivanovic, R.F., Montenegro, A., 2016. The climate response of the Indo-Pacific warm pool to glacial sea level. *Paleoceanography* 31, 866–894.
- Donohoe, A., Marshall, J., Ferreira, D., McGee, D., 2013. The relationship between ITCZ location and cross-equatorial atmospheric heat transport: from the seasonal cycle to the Last Glacial Maximum. *J. Clim.* 26, 3597–3618.
- Dufresne, J.-L., Foujols, M.-A., Denvil, S., Caubel, A., Marti, O., Aumont, O., Balkanski, Y., Bekki, S., Bellenger, H., Benshila, R., Bony, S., Bopp, L., Braconnot, P., Brockmann, P., Cadule, P., Cheruy, F., Codron, F., Cozic, A., Cugnet, D., Noblet, N., Duvel, J.-P., Ethé, C., Fairhead, L., Fichefet, T., Flavoni, S., Friedlingstein, P., Grandpeix, J.-Y., Guez, L., Guilyardi, E., Hauglustaine, D., Hourdin, F., Idelkadi, A., Ghattas, J., Joussaume, S., Kageyama, M., Krinner, G., Labetoulle, S., Lahellec, A., Lefevre, M.-F., Lefevre, F., Levy, C., Li, Z.X., Lloyd, J., Lott, F., Madec, G., Mancip, M., Marchand, M., Masson, S., Meurdésorff, Y., Mignot, J., Musat, I., Parouty, S., Polcher, J., Rio, C., Schulz, M., Swingedouw, D., Szopa, S., Talander, C., Terray, P., Viovy, N., Vuichard, N., 2013. Climate change projections using the IPSL-CM5 Earth system model: from CMIP3 to CMIP5. *Clim. Dyn.* 40, 2123–2165.
- Peakins, S.J., Sessions, A.L., 2010. Controls on the D/H ratios of plant leaf waxes in an arid ecosystem. *Geochim. Cosmochim. Acta* 74, 2128–2141.
- Fleitmann, D., Burns, S.J., Mudelsee, M., Neff, U., Kramers, J., Mangini, A., Matter, A., 2003. Holocene forcing of the Indian monsoon recorded in a stalagmite from southern Oman. *Science* (80-) 17, 1737–1739.
- Foerster, V., Junginger, A., Langkamp, O., Gebru, T., Asrat, A., Umer, M., Lamb, H.F., Wennrich, V., Rethemeyer, J., Nowaczyk, N., Trauth, M.H., Schaebitz, F., 2012. Climatic change recorded in the sediments of the Chew Bahir basin, southern Ethiopia, during the last 45,000 years. *Quat. Int.* 274, 25–37.
- Garcin, Y., Junginger, A., Melnick, D., Olago, D.O., Strecker, M.R., Trauth, M.H., 2009. Late Pleistocene–Holocene rise and collapse of lake Suguta, northern Kenya Rift. *Quat. Sci. Rev.* 28, 911–925.
- Garcin, Y., Melnick, D., Strecker, M.R., Olago, D., Tiercelin, J.-J., 2012. East African mid-Holocene wet–dry transition recorded in palaeo-shorelines of Lake Turkana, northern Kenya Rift. *Earth Planet. Sci. Lett.* 331–332, 322–334.
- Garcin, Y., Vincens, A., Williamson, D., Guiot, J., Buchet, G., 2006. Wet phases in tropical southern Africa during the last glacial period. *Geophys. Res. Lett.* 33, L07703.
- Gasse, F., Chalié, F., Vincens, A., Williams, M.A.J., Williamson, D., 2008. Climatic patterns in equatorial and southern Africa from 30,000 to 10,000 years ago reconstructed from terrestrial and near-shore proxy data. *Quat. Sci. Rev.* 27, 2316–2340.
- Gasse, F., van Campo, E., 2001. Late Quaternary environmental changes from a pollen and diatom record in the southern tropics (Lake Tritriva, Madagascar). *Palaeogeogr. Palaeoclimatol. Palaeoecol.* 167, 287–308.
- Gent, P.R., Danabasoglu, G., Donner, L.J., Holland, M.M., Hunke, E.C., Jayne, S.R., Lawrence, D.M., Neale, R.B., Rasch, P.J., Vertenstein, M., Worley, P.H., Yang, Z.-L., Zhang, M., 2011. The community climate system model version 4. *J. Clim.* 24, 4973–4991.
- Giorgetta, M.A., Jungclaus, J., Reick, C.H., Legutke, S., Bader, J., Böttger, M., Brovkin, V., Crucifix, T., Esch, M., Fieg, K., Glushak, K., Gayler, V., Haak, H., Hollweg, H.-D., Ilyina, T., Kinne, S., Kornblueh, L., Matei, D., Mauritsen, T., Mikolajewicz, U., Mueller, W., Notz, D., Pithan, F., Raddatz, T.J., Rast, S., Redler, R., Roeckner, E., Schmidt, H., Schnur, R., Segschneider, J., Six, K.D., Stockhausen, M., Timmreck, C., Wegner, J., Widmann, H., Wiemers, K.-H., Claussen, M., Marotzke, J., Stevens, B., 2013. Climate and carbon cycle changes from 1850 to 2100 in MPI-ESM simulations for the Coupled Model Intercomparison Project phase 5. *J. Adv. Model. Earth Syst.* 5, 572–597.
- Guo, Z.T., Zhou, X., Wu, H., 2012. Glacial-interglacial water cycle, global monsoon and atmospheric methane changes. *Clim. Dyn.* 39, 1073–1092.
- Hargreaves, J.C., Annan, J.D., Ohgaito, R., Paul, A., Abe-Ouchi, A., 2013. Skill and reliability of climate model ensembles at the Last Glacial Maximum and mid-Holocene. *Clim. Past.* 9, 811–823.
- Harrison, S.P., Bartlein, P.J., Izumi, K., Li, G., Annan, J.D., Hargreaves, J.C., Braconnot, P., Kageyama, M., 2015. Evaluation of CMIP5 palaeo-simulations to improve climate projections. *Nat. Clim. Chang.* 5, 735–743.
- Harrison, S.P., Jolly, D., Laarif, F., Abe-Ouchi, A., Dong, B., Herterich, K., Hewitt, C.D., Joussaume, S., Kutzbach, J.E., Mitchell, J.F.B., De Noblet, N., Valdes, P., 1998. Intercomparison of simulated global vegetation distributions in response to 6 kyr BP orbital forcing. *J. Clim.* 11, 2721–2742.
- Hastenrath, S., 2000. Zonal circulations over the equatorial Indian Ocean. *J. Clim.* 13, 2746–2756.
- Hastenrath, S., 2001. Variations of East African climate during the past two centuries. *Clim. Change* 50, 209–217.
- Hijmans, R.J., Cameron, S.E., Parra, J.L., Jones, P.G., Jarvis, A., 2005. Very high resolution interpolated climate surfaces for global land areas. *Int. J. Climatol.* 25, 1965–1978.
- Holmgren, K., Lee-Thorp, J.A., Cooper, G.R.J., Lundblad, K., Partridge, T.C., Scott, L., Sthaldeen, R., Talma, A.S., Tyson, P.D., 2003. Persistent millennial-scale climatic variability over the past 25,000 years in Southern Africa. *Quat. Sci. Rev.* 22, 2311–2326.
- Hou, J., D'Andrea, W.J., Huang, Y., 2008. Can sedimentary leaf waxes record D/H ratios of continental precipitation? Field, model, and experimental assessments. *Geochim. Cosmochim. Acta* 72, 3503–3517.
- IPCC, 2010. Good practice guidance paper on assessing and combining multi model climate projections. In: Stocker, T.F., Qin, D., Plattner, G.-K., Tignor, M., Midgley, P.M. (Eds.), *IPCC Expert Meeting on Assessing and Combining Multi Model Climate Projections*. Bern, Switzerland, p. 117pp.
- Jeffrey, S.J., Rotstayn, L.D., Collier, M., Dravitzki, S.M., Hamalainen, C., Moeseneder, C., Wong, K.K., Syktus, J.I., 2013. Australia's CMIP5 submission using the CSIRO-Mk3.6 model. *Aust. Meteorol. Oceanogr. J.* 63, 1–13.
- Jiang, D., Tian, Z., Lang, X., 2015a. Mid-Holocene global monsoon area and precipitation from PMIP simulations. *Clim. Dyn.* 44, 2493–2512.
- Jiang, D., Tian, Z., Lang, X., Kageyama, M., Ramstein, G., 2015b. The concept of global monsoon applied to the last glacial maximum: a multi-model analysis. *Quat. Sci. Rev.* 126, 126–139.
- Joussaume, S., Braconnot, P., 1997. Sensitivity of paleoclimate simulation results to season definitions. *J. Geophys. Res.* 102, 1943–1956.
- Joussaume, S., Taylor, K.E., 1995. Status of the paleoclimate modeling intercomparison project (PMIP). *World Meteorol. Organ* 425–430. TD.
- Joussaume, S., Taylor, K.E., Braconnot, P., Mitchell, J.F.B., Kutzbach, J.E., Harrison, S.P., Prentice, I.C., Broccoli, A.J., Abe-Ouchi, A., Bartlein, P.J., Bonfigli, C., Dong, B., Guiot, J., Herterich, K., Hewitt, C.D., Jolly, D., Kim, J.W., Kislov, A., Kitoh, A., Loutre, M.-F., Masson-Delmotte, V., McAvaney, B., McFarlane, N., De Noblet, N., Peltier, W.R., Peterschmitt, J., Pollard, D., Rind, D., Royer, J.F., Schlesinger, M.E., Syktus, J.I., Thompson, S., Valdes, P., Vettoretti, G., Webb, R.S., Wypatta, U., 1999. Monsoon changes for 6000 years ago: results of 18 simulations from the paleoclimate modeling intercomparison project (PMIP). *Geophys. Res. Lett.* 26, 859–862.
- Jungclaus, J., Keenlyside, N., Botzet, M., Haak, H., Luo, J.-J., Latif, M., Marotzke, J., Mikolajewicz, U., Roeckner, E., 2006. Ocean circulation and tropical variability in the coupled model ECHAM5/MPI-OM. *J. Clim.* 19, 3952–3972.
- Kalnay, E., Kanamitsu, M., Kistler, R., Collins, W.D., Deaven, D., Gandin, L., Iredell, M., Saha, S., White, G., Woollen, J., Zhu, Y., Chelliah, M., Ebisuzaki, W., Higgins, W., Janowiak, J., Mo, K.C., Ropelewski, C., Wang, J., Leetmaa, A., Reynolds, R., Jenne, R., Joseph, D., 1996. The NCEP/NCAR 40-years reanalysis Project. *Bull. Am. Meteorol. Soc.* 77, 437–471.
- Knutti, R., Furrer, R., Tebaldi, C., Cermak, J., Meehl, G.A., 2010. Challenges in combining projections from multiple climate models. *J. Clim.* 23, 2739–2758.
- Konecky, B.L., Russell, J.M., Johnson, T.C., Brown, E.T., Berke, M.A., Werne, J.P., Huang, Y., 2011. Atmospheric circulation patterns during late Pleistocene climate changes at Lake Malawi, Africa. *Earth Planet. Sci. Lett.* 312, 318–326.
- Kutzbach, J.E., 1981. Monsoon climate of Early Holocene: climate experiment with the Earth's Orbital parameters for 9000 years ago. *Science* (80-) 214, 59–61.
- Kutzbach, J.E., Street-Perrott, F.A., 1985. Milankovitch forcing of fluctuations in the level of tropical lakes from 18 to 0 kyr BP. *Nature* 317, 130–134.
- Li, L., Lin, P., Yu, Y., Wang, B., Zhou, T., Liu, L., Liu, J., Bao, Q., Xu, S., Huang, W., Xia, K., Pu, Y., Dong, L., Shen, S., Liu, Y., Hu, N., Liu, M., Sun, W., Shi, X., Zheng, W., Wu, B., Song, M., Liu, H., Zhang, X., Wu, G., Xue, W., Huang, X., Yang, G., Song, Z., Qiao, F., 2013. The flexible global ocean-atmosphere-land system model, Grid-point Version 2: FGOALS-g2. *Adv. Atmos. Sci.* 30, 543–560.
- Lim, S., Chase, B.M., Chevalier, M., Reimer, P.J., 2016. 50,000 years of climate in the Namib desert, Pella, South Africa. *Palaeogeogr. Palaeoclimatol. Palaeoecol.* 451, 197–209.
- Loomis, S.E., Russell, J.M., Ladd, B., Street-Perrott, F.A., Sinnenberg Damsté, J.S., 2012. Calibration and application of the branched GDGT temperature proxy on East African lake sediments. *Earth Planet. Sci. Lett.* 357–358, 277–288.
- Marshall, M.H., Lamb, H.F., Huws, D., Davies, S.J., Bates, R., Bloemendal, J., Boyle, J., Leng, M.J., Umer, M., Bryant, C., 2011. Late Pleistocene and Holocene drought events at lake Tana, the source of the blue Nile. *Glob. Planet. Change* 78, 147–161.
- McCarroll, D., 2015. "Study the past, if you would divine the future": a retrospective on measuring and understanding Quaternary climate change. *J. Quat. Sci.* 30, 154–187.
- McDermott, F., 2004. Palaeo-climate reconstruction from stable isotope variations in speleothems: a review. *Quat. Sci. Rev.* 23, 901–918.
- McGee, D., Donohoe, A., Marshall, J., Ferreira, D., 2014. Changes in ITCZ location and cross-equatorial heat transport at the last glacial maximum, Heinrich Stadial 1, and the mid-Holocene. *Earth Planet. Sci. Lett.* 390, 69–79.
- Neumann, F.H., Botha, G.A., Scott, L., 2014. 18,000 years of grassland evolution in the

- summer rainfall region of South Africa: evidence from Mahwaqa Mountain, KwaZulu-Natal. *Veg. Hist. Archaeobot* 23, 665–681.
- Neumann, F.H., Scott, L., Bousman, C.B., van As, L., 2010. A Holocene sequence of vegetation change at Lake Eteza, coastal KwaZulu-Natal, South Africa. *Rev. Palaeobot. Palynol.* 162, 39–53.
- Neumann, F.H., Stager, J.C., Scott, L., Venter, H.J.T., Weyhenmeyer, C., 2008. Holocene vegetation and climate records from lake Sibaya, KwaZulu-Natal (South Africa). *Rev. Palaeobot. Palynol.* 152, 113–128.
- Nicholson, S.E., 2015. Long-term variability of the East African “short rains” and its links to large-scale factors. *Int. J. Climatol.* 35, 3979–3990.
- Norström, E., Neumann, F.H., Scott, L., Smittenberg, R.H., Holmstrand, H., Lundqvist, S., Snowball, I., Sundqvist, H., Risberg, J., Bamford, M.K., 2014. Late Quaternary vegetation dynamics and hydro-climate in the Drakensberg, South Africa. *Quat. Sci. Rev.* 105, 48–65.
- Otto-Blaeser, B.L., Russell, J.M., Clark, P.U., Liu, Z., Overpeck, J.T., Konecky, B.L., DeMenocal, P.B., Nicholson, S.E., He, F., Lu, Z., 2014. Coherent changes of southeastern equatorial and northern African rainfall during the last deglaciation. *Science* (80–) 346, 1223–1227.
- Partin, J.W., Cobb, K.M., Banner, J.L., 2008. Climate variability recorded in tropical and sub-tropical speleothems. *PAGES News* 16, 9–10.
- Perez-Sanz, A., Li, G., González-Sampériz, P., Harrison, S.P., 2014. Evaluation of modern and mid-Holocene seasonal precipitation of the Mediterranean and northern Africa in the CMIP5 simulations. *Clim. Past.* 10, 551–568.
- Peyron, O., Jolly, D., Braconnot, P., Bonnefille, R., Guiot, J., Wirrmann, D., Chalié, F., 2006. Quantitative reconstructions of annual rainfall in Africa 6000 years ago: model-data comparison. *J. Geophys. Res.* 111, 1–9.
- Hippis, S.J., Rotstain, L.D., Gordon, H.B., Roberts, J.L., Hirst, A.C., Budd, W.F., 2011. The CSIRO Mk3L climate system model version 1.0 – Part 1: description and evaluation. *Geosci. Model Dev.* 4, 483–509.
- Hippis, S.J., Rotstain, L.D., Gordon, H.B., Roberts, J.L., Hirst, A.C., Budd, W.F., 2012. The CSIRO Mk3L climate system model version 1.0 – Part 2: response to external forcings. *Geosci. Model Dev.* 5, 649–682.
- Pinot, S., Ramstein, G., Harrison, S.P., Prentice, I.C., Guiot, J., Stute, M., Joussaume, S., 1999. Tropical paleoclimates at the last glacial maximum: comparison of paleoclimate modeling intercomparison project (PMIP) simulations and paleodata. *Clim. Dyn.* 15, 857–874.
- Prell, W.L., Kutzbach, J.E., 1987. Monsoon variability over the past 150,000 years. *J. Geophys. Res.* 92, 8411–8425.
- Quick, L.J., Carr, A.S., Meadows, M.E., Boom, A., Bateman, M.D., Roberts, D.L., Reimer, P.J., Chase, B.M., 2015a. A late Pleistocene-Holocene multi-proxy record of palaeoenvironmental change from Still Bay, southern Cape Coast, South Africa. *J. Quat. Sci.* 30, 870–885.
- Quick, L.J., Meadows, M.E., Bateman, M.D., Kirsten, K.L., Mäusbacher, R., Haberzettl, T., Chase, B.M., 2015b. Vegetation and climate dynamics during the last glacial period in the fynbos-afrotropical forest ecotone, southern Cape, South Africa. *Quat. Int.* 30 (1), e14.
- Raddatz, T.J., Reick, C.H., Knorr, W., Kattge, J., Roeckner, E., Schnur, R., Schnitzler, K.G., Wetzel, P., Jungclaus, J., 2007. Will the tropical land biosphere dominate the climate-carbon cycle feedback during the twenty-first century? *Clim. Dyn.* 29, 565–574.
- Reynolds, R.W., Rayner, N.A., Smith, T.M., Stokes, D.C., Wang, W., 2002. An improved in situ and satellite SST analysis for climate. *J. Clim.* 15, 1609–1625.
- Roeckner, E., Bäuml, G., Bonaventura, L., Brokopf, R., Esch, M., Giorgetta, M., Hagemann, S., Kirchner, I., Kornblueh, L., Rhodin, A., Schlese, U., Schulzweida, U., Tompkins, A., 2003. The atmospheric general circulation model ECHAM5: Part 1: model description. *Rep./MPI für Meteorol.* 349, 1–140.
- Rotstain, L.D., Jeffrey, S.J., Dravitzki, S.M., Hirst, A.C., Syktus, J.I., Wong, K.K., 2012. Aerosol- and greenhouse gas-induced changes in summer rainfall and circulation in the Australasian region: a study using single-forcing climate simulations. *Atmos. Chem. Phys.* 12, 6377–6404.
- Schefuß, E., Kuhlmann, H., Mollenhauer, G., Prange, M., Pätzold, J., 2011. Forcing of wet phases in southeast Africa over the past 17,000 years. *Nature* 480, 509–512.
- Schefuß, E., Schouten, S., Schneider, R.R., 2005. Climatic controls on central African hydrology during the past 20,000 years. *Nature* 437, 1003–1006.
- Schmidt, G.A., Annan, J.D., Bartlein, P.J., Cook, B.I., Guiyardi, E., Hargreaves, J.C., Harrison, S.P., Kageyama, M., Legrande, A.N., Konecky, B.L., Lovejoy, S., Mann, M.E., Masson-Delmotte, V., Risi, C., Thompson, D., Timmermann, A., You, P., 2014a. Using palaeo-climate comparisons to constrain future projections in CMIP5. *Clim. Past.* 10, 221–250.
- Schmidt, G.A., Kelley, M., Nazarenko, L., Ruedy, R., Russell, G.L., Aleinov, I., Bauer, M., Bauer, S.E., Bhat, M.K., Bleck, R., Canuto, V., Chen, Y., Cheng, Y., Clune, T.L., Del Genio, A., de Fainchtein, R., Faluvegi, G., Hansen, J.E., Healy, R.J., Kiang, N.Y., Koch, D., Lacis, A.A., Legrande, A.N., Lerner, J., Lo, K.K., Matthews, E.E., Menon, S., Miller, R.L., Oinas, V., Oloso, A.O., Perlitz, J.P., Puma, M.J., Putman, W.M., Rind, D., Romanou, A., Sato, M., Shindell, D.T., Sun, S., Syed Rahman, A., Tausnev, N., Tsigaridis, K., Under, N., Voulgarakis, A., Yao, M.-S., Zhang, J., 2014b. Configuration and assessment of the GISS ModelE2 contributions to the CMIP5 archive. *J. Adv. Model. Earth Syst.* 6, 141–184.
- Schneider, T., Bischoff, T., Haug, G.H., 2014. Migrations and dynamics of the inter-tropical convergence zone. *Nature* 513, 45–53.
- Schulzweida, U., Kornblueh, L., Quast, R., 2014. CDO: Climate Data Operators v1.6.4. Cent. Mar. Atmos. Sci. (ZMAW). Max-Planck Inst. Meteorol. Univ. Hamburg. <https://code.zmau.de/projects/cdo> (last access August 2014).
- Scott, L., Neumann, F.H., Brook, G.A., Bousman, C.B., Norström, E., Metwally, A.A.S.A.H., 2012. Terrestrial fossil-pollen evidence of climate change during the last 26 thousand years in Southern Africa. *Quat. Sci. Rev.* 32, 100–118.
- Shakun, J.D., Burns, S.J., Fleitmann, D., Kramers, J., Matter, A., Al-Subary, A., 2007. A high-resolution, absolute-dated deglacial speleothem record of Indian Ocean climate from Socotra Island, Yemen. *Earth Planet. Sci. Lett.* 259, 442–456.
- Singarayer, J.S., Burrough, S.L., 2015. Interhemispheric dynamics of the African rainbelt during the late Quaternary. *Quat. Sci. Rev.* 124, 48–67.
- Sinninghe Damsté, J.S., Verschuren, D., Ossebaar, J., Blokker, J., van Houten, R., van der Meer, M.T.J., Plessen, B., Schouten, S., 2011. A 25,000-year record of climate-induced changes in lowland vegetation of eastern equatorial Africa revealed by the stable carbon-isotopic composition of fossil plant leaf waxes. *Earth Planet. Sci. Lett.* 302, 236–246.
- Sonzogni, C., Bard, E., Rostek, F., 1998. Tropical sea-surface temperatures during the last glacial period: a view based on alkenones in Indian Ocean sediments. *Quat. Sci. Rev.* 17, 1185–1201.
- Sueyoshi, T., Ohgaito, R., Yamamoto, A., Chikamoto, M.O., Hajima, T., Okajima, H., Yoshimori, M., Abe, M., Oishi, R., Saito, F., Watanabe, S., Kawamiya, M., Abe-Ouchi, A., 2013. Set-up of the PMIP3 paleoclimate experiments conducted using an Earth system model, MIROC-ESM. *Geosci. Model Dev.* 6, 819–836.
- Taylor, K.E., Stouffer, R.J., Meehl, G.A., 2012. An overview of CMIP5 and the experiment design. *Bull. Am. Meteorol. Soc.* 93, 485–498.
- Tierney, J.E., DeMenocal, P.B., 2013. Abrupt shifts in Horn of Africa hydroclimate since the last glacial maximum. *Sci.* (80–) 342, 843–846.
- Tierney, J.E., Lewis, S.C., Cook, B.I., LeGrande, A.N., Schmidt, G.A., 2011a. Model, proxy and isotopic perspectives on the east African humid period. *Earth Planet. Sci. Lett.* 307, 103–112.
- Tierney, J.E., Russell, J.M., Huang, Y., Sinninghe Damsté, J.S., Hopmans, E.C., Cohen, A.S., 2008. Northern hemisphere controls on tropical southeast African climate during the past 60,000 years. *Science* (80–) 322, 252–255.
- Tierney, J.E., Russell, J.M., Sinninghe Damsté, J.S., Huang, Y., Verschuren, D., 2011b. Late quaternary behavior of the east African monsoon and the importance of the Congo air boundary. *Quat. Sci. Rev.* 30, 798–807.
- Truc, L., Chevalier, M., Favier, C., Cheddadi, R., Meadows, M.E., Scott, L., Carr, A.S., Smith, G.F., Chase, B.M., 2013. Quantification of climate change for the last 20,000 years from Wonderkrater, South Africa: implications for the long-term dynamics of the Intertropical Convergence Zone. *Palaeogeogr. Palaeoclimatol. Palaeoecol.* 386, 575–587.
- Verschuren, D., Sinninghe Damsté, J.S., Moernaut, J., Kristen, I., Blaauw, M., Fagot, M., Haug, G.H., 2009. Half-precessional dynamics of monsoon rainfall near the East African Equator. *Nature* 462, 637–641.
- Voldoire, A., Sanchez-Gomez, E., Salas y Méliá, D., Decharme, B., Cassou, C., Sénési, S., Valcke, S., Beau, I., Alias, A., Chevallier, M., Déqué, M., Deshayes, J., Douville, H., Fernandez, E., Madec, G., Maisonneuve, E., Moine, M.-P., Planton, S., Saint-Martin, D., Szopa, S., Tyteca, S., Alkama, R., Belamari, S., Braun, A., Coquart, L., Chauvin, F., 2012. The CNRM-CM5.1 global climate model: description and basic evaluation. *Clim. Dyn.* 40, 2091–2121.
- Wang, B., Ding, Q., 2008. Global monsoon: dominant mode of annual variation in the tropics. *Dyn. Atmos. Ocean.* 44, 165–183.
- Wang, P.X., Wang, B., Cheng, H., Falutto, J.T., Guo, Z.T., Kiefer, T., Liu, Z.Y., 2014. The global monsoon across timescales: coherent variability of regional monsoons. *Clim. Past.* 10, 2007–2025.
- Wang, Y.J., Cheng, H., Edwards, R.L., An, Z.S., Wu, J.Y., Shen, C.C., Dorale, J.A., 2001. A high-resolution absolute-dated late Pleistocene Monsoon record from Hulu Cave, China. *Science* (80–) 294, 2345–2348.
- Wang, Y.V., Larsen, T., Leduc, G., Andersen, N., Blanz, T., Schneider, R.R., 2013. What does leaf wax δD from a mixed C3/C4 vegetation region tell us? *Geochim. Cosmochim. Acta* 111, 128–139.
- Watanabe, S., Hajima, T., Sudo, K., Nagashima, T., Takemura, T., Okajima, H., Nozawa, T., Kawase, H., Abe, M., Yokohata, T., Ise, T., Sato, H., Kato, E., Takata, K., Emori, S., Kawamiya, M., 2011. MIROC-ESM 2010: model description and basic results of CMIP5-20C3M experiments. *Geosci. Model Dev.* 4, 845–872.
- Xin, X.-G., Wu, T.-W., Zhang, J., 2013. Introduction of CMIP5 experiments carried out with the climate system models of Beijing climate Center. *Adv. Clim. Chang. Res.* 4, 41–49.
- Yim, S.-Y., Wang, B., Liu, J., Wu, Z., 2014. A comparison of regional monsoon variability using monsoon indices. *Clim. Dyn.* 43, 1423–1437.
- Yukimoto, S., Adachi, Y., Hosaka, M., Sakami, T., Yoshimura, H., Hirabara, M., Tanaka, T.Y., Shindo, E., Tsujino, H., Deushi, M., Mizuta, R., Yabu, S., Obata, A., Nakano, H., Koshiro, T., Ose, T., Kitoh, A., 2012. A new global climate model of the meteorological research institute: MRI-CGCM3-model description and basic performance. *J. Meteorol. Soc. Jpn.* 90A, 23–64.